PERGAMON

International Journal of Multiphase Flow 26 (2000) 1247–1279

International Journal of Multiphase Flow

www.elsevier.com/locate/ijmulflow

Wall-bounded shear flow and channel flow of suspensions of liquid drops

Xiaofan Li[a], C. Pozrikidis[b,*]

[a]*Department of Mathematics, Ohio State University, 231 W. 18th Ave., Columbus, OH 43210, USA*
[b]*University of California, San Diego, La Jolla, CA 92093-0411, USA*

Received 20 November 1998; received in revised form 11 July 1999

Abstract

The wall-bounded shear flow and the plane Poiseuille channel flow of monodisperse suspensions of liquid drops are considered by theory and numerical simulation. First, the motion of an individual drop in infinite or semi-infinite shear flow is discussed in the limit of small volume fractions. An expression for the flux of the drops normal to the streamlines of the unperturbed flow is derived in terms of (a) the migration velocity of the drop away from the wall, and (b) the net displacement of a drop's center after interception with another drop. In the case of two-dimensional infinite shear flow, in the limit of infinite dilution, and in the context of Stokes flow, the self- and gradient-diffusivity are found to diverge, and this underlines the importance of fluid inertia and the necessity to perform renormalization by requiring global constraints. Numerical simulations of pairwise drop interceptions in semi-infinite shear flow above a plane wall reveal that the capillary number, expressing the drop deformability, and the distance of the drop pair from the wall, play an important role in determining not only the magnitude, but also the direction of the net displacement of the drop center after recession. Dynamic simulations of the expansion of a periodic bed of drops distributed randomly within a layer next to a wall illustrate explicitly the formation of a particle-free zone near the wall and the thickening of the bed due to hydrodynamic interceptions at a rate that is a strong function of the capillary number. Results of dynamic simulations of the pressure-driven flow of a two-dimensional suspension in a channel confined between two parallel walls are presented illustrating the effect of the capillary number and of the ratio of the viscosity of the drop and suspending fluid on (a) the time required for the suspension to reach statistical equilibrium, (b) the distribution of the drop number density across the channel width, (c) the mean velocity profile, and (d) the effective viscosity of the suspension. The general features of the flow are found to be in good agreement with published laboratory observations.

Keywords: Suspensions; Drops; Channel flow; Boundary integral methods

* Corresponding author.
E-mail address: cpozrikidis@ucsd.edu (C. Pozrikidis).

0301-9322/00/$ - see front matter
PII: S0301-9322(99)00087-7

1. Introduction

The shear flow of dilute and dense suspensions of liquid drops in an effectively unbounded domain has been the subject of a number of recent studies, as reviewed by Li et al. (1996), Charles and Pozrikidis (1998), and Guido and Simeone (1998). Theoretical and computational approaches can be classified into several categories depending to their objectives: investigations of single drop deformation, possibly in the presence of interfacial rheology or surfactants, with emphasis on determining the magnitude of the deformation and establishing conditions for breakup; investigations of pairwise drop interactions with emphasis on establishing conditions for drop coalescence and computing the drop displacement after interception; numerical simulations of ordered and random suspensions accompanied by theoretical analyses of the rheological properties of the suspension and of the statistics of the individual drop motion. The results provide us with fundamental insights into the industrial processes of fluid mixing, dispersion and emulsification, emulsion handling, composite material manufacturing, as well into several branches of biorheology involving blood flow.

In practice, the flow of a suspension typically occurs in a domain that is bounded by solid surfaces whose presence has a significant effect on the way in which the drops are distributed in the suspension. It is known, for example, that isolated drops, and more general deformable capsules, spontaneously migrate away from solid surfaces yielding particle-free zones. Such migration is also observed in suspensions of rigid particles, but it occurs at a slower rate and only at sufficiently high particle volume fractions: in Stokes flow, migration of perfect rigid spheres can occur only through particle interactions. When a suspension is non-dilute, or the mean shear rate varies with position in pressure-driven channel flow, there are additional motions due to inter-particle and shear gradient-particle interactions that have been described in terms of diffusive fluxes and associated hydrodynamic self- or gradient-diffusivities. The combination of these motions leads to a complex behavior that has defied accurate description in the context of continuum mechanics, and has been only amenable to phenomenological modeling.

The wall-bounded and tube flow of suspensions of rigid spheres has been considered on several occasions by theoretical analysis, numerical simulation, and laboratory observation. Recent contributions to the theory accompanied by numerical simulations were made by Nott and Brady (1994) and Morris and Brady (1998). Recent laboratory measurements were reported by Koh et al. (1994) and Hampton et al. (1997). These studies demonstrated explicitly the blunting of the mean velocity profile due to the presence of the particles, and the development of inhomogeneities in the particle number distribution due to particle accumulation at regions of low shear rate. Investigations of wall-bounded and pressure-driven flow of suspensions of liquid drops include several theoretical and computational studies of individual drop migration away from a plane wall or tube surface (e.g. Kennedy et al., 1994; Coulliette and Pozrikidis, 1998), a few laboratory observations of multi-disperse emulsions (Han and King, 1980; Kowalewski, 1980, 1984; Hiller and Kowalewski, 1987), and a limited set of numerical simulations of the shear- and pressure-driven flow in a channel confined between two parallel plane walls (Zhou and Pozrikidis, 1993a, 1993b, 1994).

In the present work, we study several aspects of the wall-bounded and channel flow of dilute and dense suspensions of liquid drops at vanishing particle Reynolds number, by theory and

numerical simulation. Since the accurate simulation of three-dimensional suspensions consisting of more than a few suspended drops is prohibited by high computational cost and the unavailability of efficient algorithms for interface tracking (e.g. Kwak and Pozrikidis, 1998), we restrict our attention to two-dimensional systems. The consequences of dropping the third dimension are not entirely known. Previous numerical simulations of the infinite shear flow of non-dilute suspensions have suggested that a number of salient rheological and statistical properties are not significantly altered. We shall see, however, that although several aspects of the present discussion for two-dimensional flow can be extended to three-dimensional flow by straightforward generalization, some differences arise in the limit of infinite dilution.

In Section 2, we discuss the motion of an individual drop in an infinite or semi-infinite dilute suspension bounded by a plane wall in terms of the velocity induced by the wall and the drop number density flux due to pairwise interactions. An attempt to express the flux of the particle number density in terms of a self- or gradient-diffusivity leads to divergent integrals owing to the slow decay of disturbances in Stokes flow. This singular behavior underlines the importance of fluid inertia and points to the need for renormalization by requiring global constraints. In Section 3, we present numerical simulations of the flow-induced expansion of a bed of drops next to a wall and demonstrate explicitly the formation of a drop-free zone. The results allow us to estimate the rate of thickening of the bed due to multiple drop interceptions.

In the second part of this paper, we consider the internal flow of a suspension in a channel, where the motion is driven by an imposed pressure gradient. In this case, in addition to the drop number density flux due to the wall-induced migration velocity, there is an additional flux associated with particle motions normal to the streamlines of the unperturbed flow due to the spatial variation of the macroscopic shear rate. In the absence of a convenient model for studying the latter in isolation, we consider the full problem of channel flow and analyze the structure of the suspension after hydrodynamic equilibrium has established. In the numerical studies, we simulate the pressure-driven flow of a periodic suspension in a channel that is confined by two parallel plane walls, thus extending the previous simulations by Zhou and Pozrikidis (1994) to a higher number of drops and to viscosity ratios other than unity. The first extension allows us to discuss the statistics of the motion, which was not possible in the earlier study. The second extension allows us to explicitly demonstrate the change in the nature of the flow as the viscosity of the suspended phase is raised and the liquid drops effectively behave as rigid particles.

2. Evolution of the drop number density distribution in shear flow

Consider the simple shear flow of a monodisperse suspension of neutrally buoyant, two-dimensional drops with viscosity $\lambda\mu$, dispersed in ambient fluid with viscosity μ, with the interfaces exhibiting constant surface tension γ, as illustrated in Fig. 1(a). The suspension is bounded on one side by a stationary infinite plane wall that is parallel to the x-axis, and extends to infinity in the positive direction of the y-axis. Assuming that the drop distribution remains statistically homogeneous with respect to x at all times, we seek an equation that describes the evolution of the spatial distribution of the drop centroids, expressed in terms of

the drop number density n which is defined as the number of drops per unit area of the suspension. The assumption of homogeneity in the streamwise direction allows us to regard n a function of distance from the wall and time, $n(y, t)$.

2.1. Drop migration

In the limit of infinite dilution, each drop is advected and deforms under the action of the shear flow as though it were in isolation. A number of previous studies have shown that a deformable two- or three-dimensional drop slowly migrates away from the wall at a rate that is a function of the capillary number $Ca = \mu G a/\gamma$, the viscosity ratio λ, and the distance of the drop centroid from the wall (e.g. Kennedy et al., 1994); G is the shear rate of the mean shear flow, and a is the equivalent drop radius. Unless the drop is very viscous, the rate of migration away from the wall is significantly smaller than the rate of change of the drop shape, and the motion is quasi-steady. The velocity of the drop centroid normal to the wall, in the direction of the y-axis, may thus be expressed as

$$v_y^\infty = G\, a\, \hat{v}_y^\infty \left(Ca, \lambda, \frac{y_c}{a} \right) \tag{1}$$

where $\hat{v}_y^\infty$ is a dimensionless function of its arguments, a caret designates a dimensionless variable, and y_c is the instantaneous distance of the drop centroid from the wall. Reversibility of Stokes flow requires that in the limit as Ca tends to zero, the migration velocity $\hat{v}_y^\infty$ vanish. The flux of the drop number density along the y-axis due to the wall is given by

$$j_y^\infty(y, t) = n(y, t)\ v_y^\infty = G\, a\, n(y, t) \hat{v}_y^\infty \left(Ca, \lambda, \frac{y}{a} \right) \tag{2}$$

It is physically appealing to attribute the flux j_y^∞ to a flow-induced hydrodynamic potential generated by the wall. The strength of this potential decays rapidly with distance from the wall, and effectively vanishes at a distance that is equal to several drop radii away from the wall. If the drops were not neutrally buoyant, there would be an additional flux due to the gravitational potential involving the mobility of the drops in the presence of the wall. When the gravity-induced motion drives the drops toward the wall, equilibrium conditions will exist in certain ranges of Ca and λ where the settling velocity balances the shear-induced migration velocity, and the drops concentrate and translate steadily at a certain distance above the wall.

2.2. Pairwise interactions

As long as the drop number density is non-zero, however small, one drop occasionally intercepts other drops in the evolving suspension. Assuming, as a first approximation, that the drops are advected with the velocity of the unperturbed simple shear flow, we find that the rate of interception of a test drop whose center is located at y, with another drop whose center lies within a horizontal strip of width $\mathrm{d}y'$ centered at y', is given by

$$r(y, y') = G|y - y'|n(y', t)\, \mathrm{d}y' \tag{3}$$

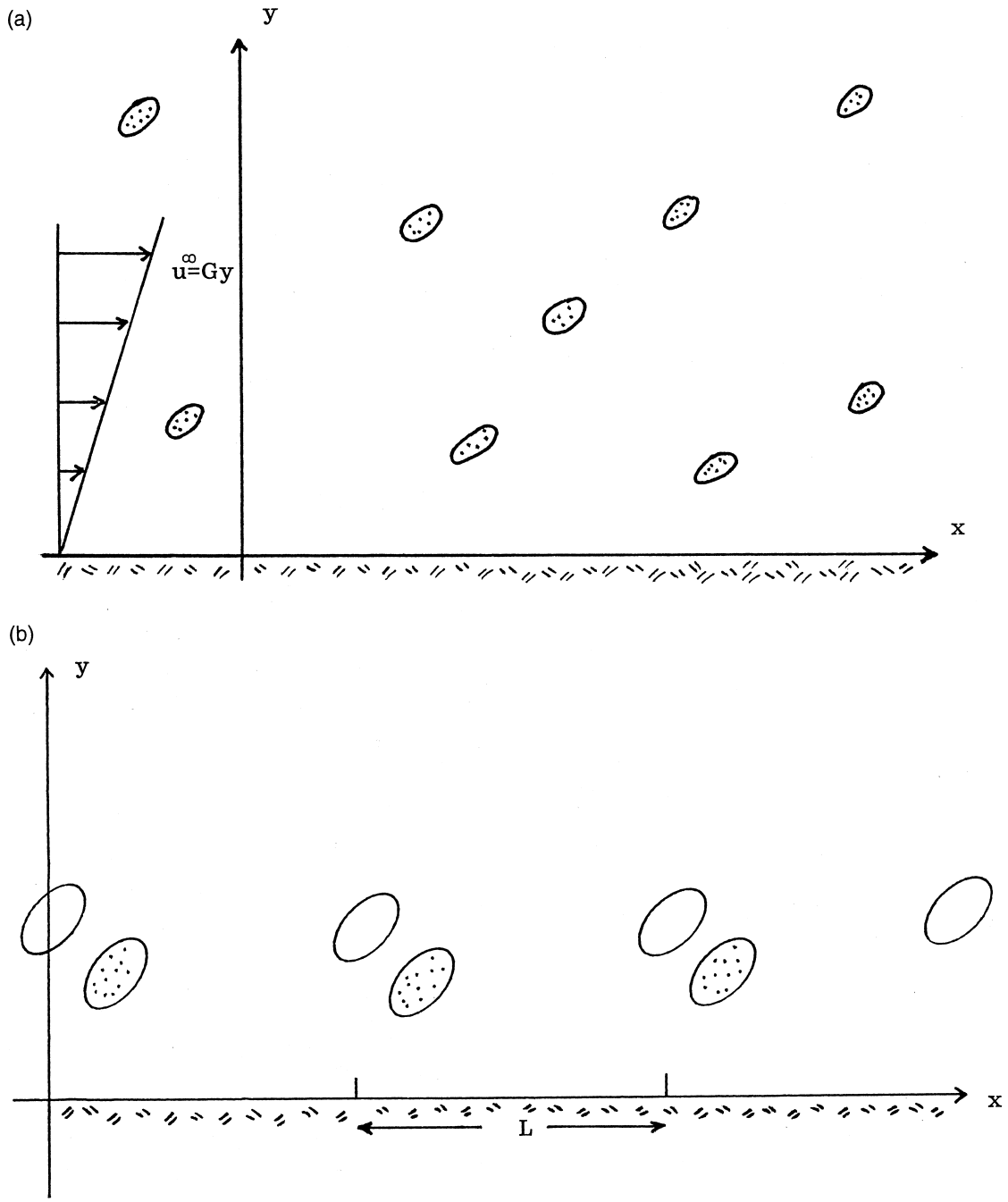

Fig. 1. Illustration of (a) a semi-infinite suspension of two-dimensional liquid drops in simple shear flow, bounded on one side by a plane wall and extending to infinity on the other side; (b) a semi-infinite periodic suspension consisting of two arrays of drops, serving as a model for studying pairwise drop interceptions in a dilute suspension.

Both y and y' vary over the range $(y_{\min}, \infty)$, where the minimum distance from the wall at which a drop center can be found, $y_{\min}$, is comparable to the drop radius. In the theoretical limit of zero capillary number, the drops are circular and $y_{\min}$ is equal to the drop radius. After recession, the test drop has undergone a positive or negative net displacement along the y-axis, which we denote as $\delta(y, y') = y_{\text{After}} - y$. In Section 2.4, we shall present results of numerical simulations illustrating the dependence of $\delta(y, y')$ on the distance of each one of two drops from the wall.

2.3. Pairwise interactions in infinite shear flow

Before considering the motion in the presence of wall, we discuss the simpler case of infinite shear flow in the absence of a wall. In this case, the lower limit $y_{\min}$ is shifted to $-\infty$, and the net displacement $\delta(y, y')$ is an odd function of the drop distance $\Delta y = y - y'$. Charles and Pozrikidis (1998) presented graphs of δ versus the viscosity ratio and capillary number for a particular value of $\Delta y/a$. da Cunha and Hinch (1996) and Loewenberg and Hinch (1997) presented lattice graphs of $\delta(\Delta y, \Delta z)$ for rough spheres and three-dimensional drops with repulsive interfacial forces included to prevent coalescence; Δz is the initial particle separation in the direction of the vorticity of the simple shear flow.

To illustrate the functional form of $\delta(\Delta y)$, we simulated the motion of two initially circular drops that are separated by the negative streamwise distance $-\Delta x = x - x'$, up to the point where the drops have intercepted and separated by the positive distance Δx. Fig. 2(a) displays graphs of the lateral drop position of one intercepting drop with respect to time for $\Delta x/a = 20$, and Fig. 2(b) and (c) display graphs of $\delta(\Delta y)$ on linear and logarithmic scales for several values of $\Delta x/a$, all for $\lambda = 1$ and $Ca = 0.1$. It is most significant to note that, as $|\Delta x|/a$ tends to infinity, the tail of $\delta(\Delta y)$ decays like Δy^{-1}, which is consistent with the fact that, because the drops are neutrally buoyant, the velocity generated in the vicinity of one drop by the other drop resembles the flow due to a two-dimensional point-force dipole that is inclined at a certain angle with respect to the direction of the unperturbed shear flow. At large separations, the yy component of the dipole determines the motion across the streamlines of the unperturbed flow. For well-separated drops, the strength and direction of the dipole may be approximated with the steady values corresponding to a solitary drop suspended in simple shear flow.

Next, we observe that when the drop number density distribution is uniform and equal to n over a region that is large compared to the equivalent drop radius, a drop may experience a large number of interceptions while remaining in its initial environment. Under the fundamental assumption that the interceptions are uncorrelated, we may use the theory of random walks to describe the motion due to pairwise interceptions in terms of the long-time self-diffusivity D^s defined in terms of the dispersion in the lateral position of a drop after a large number of interceptions (e.g. Rief, 1965, pp. 32–35). Noting that the mean value of the displacement vanishes due to symmetry, and assuming that strongly interacting drops that are initially separated by a small distance do not coalesce, we find

$$D^s = \frac{1}{2}\int_{-\infty}^{\infty} \delta^2(\Delta y) r(y, y')\, \mathrm{d}\Delta y = G\, n \int_0^{\infty} \delta^2(\Delta y)|\Delta y|\, \mathrm{d}\Delta y \tag{4}$$

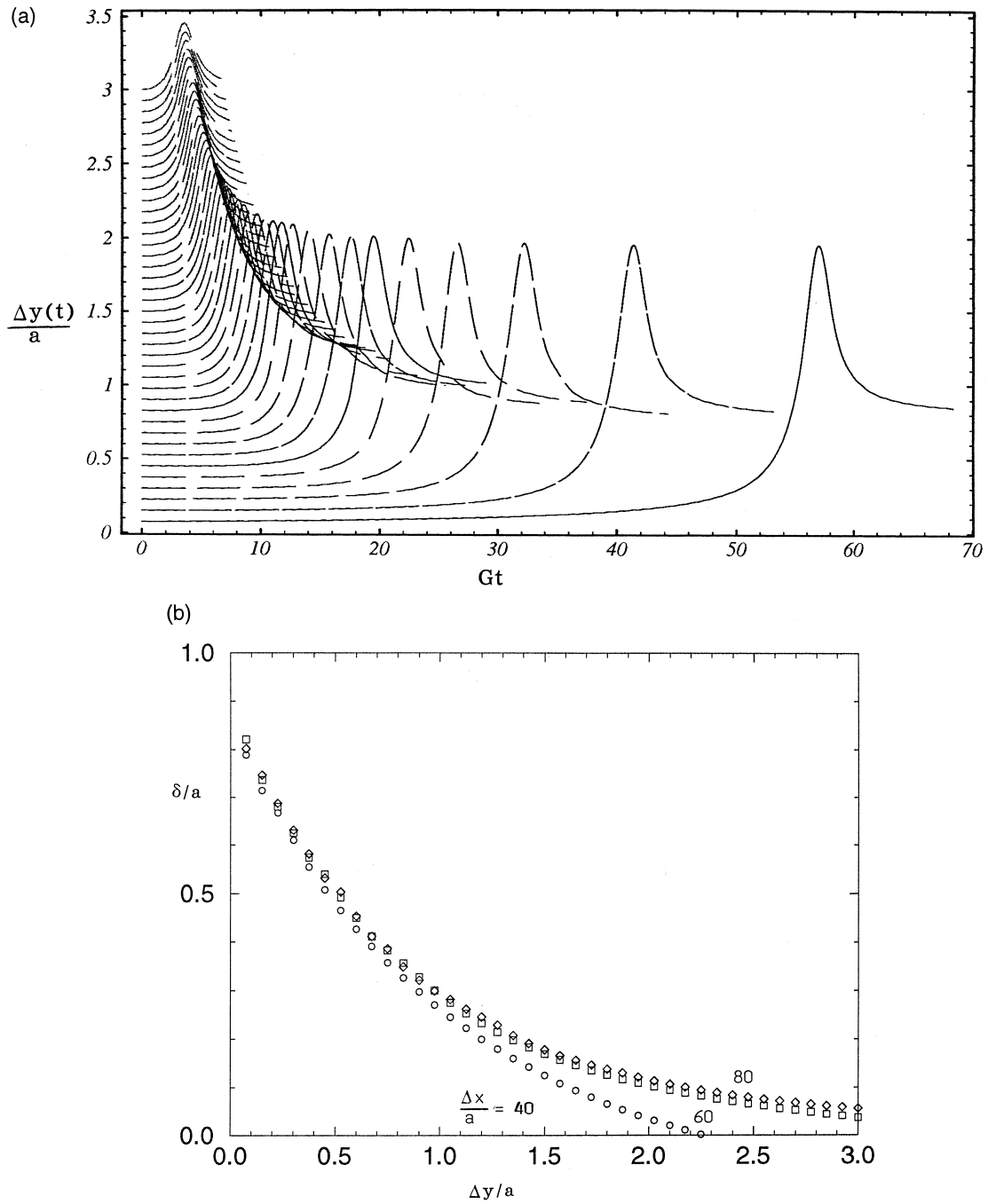

Fig. 2. (a) Evolution of the lateral position of a drop interacting with another drop in infinite shear flow with shear rate G, for $\lambda = 1$ and $Ca = 0.1$, initial separation $\Delta x = 20a$, and various initial lateral displacements Δy. (b, c) Net displacement of a drop after interception with another drop in infinite simple shear flow, for various initial separations Δx.

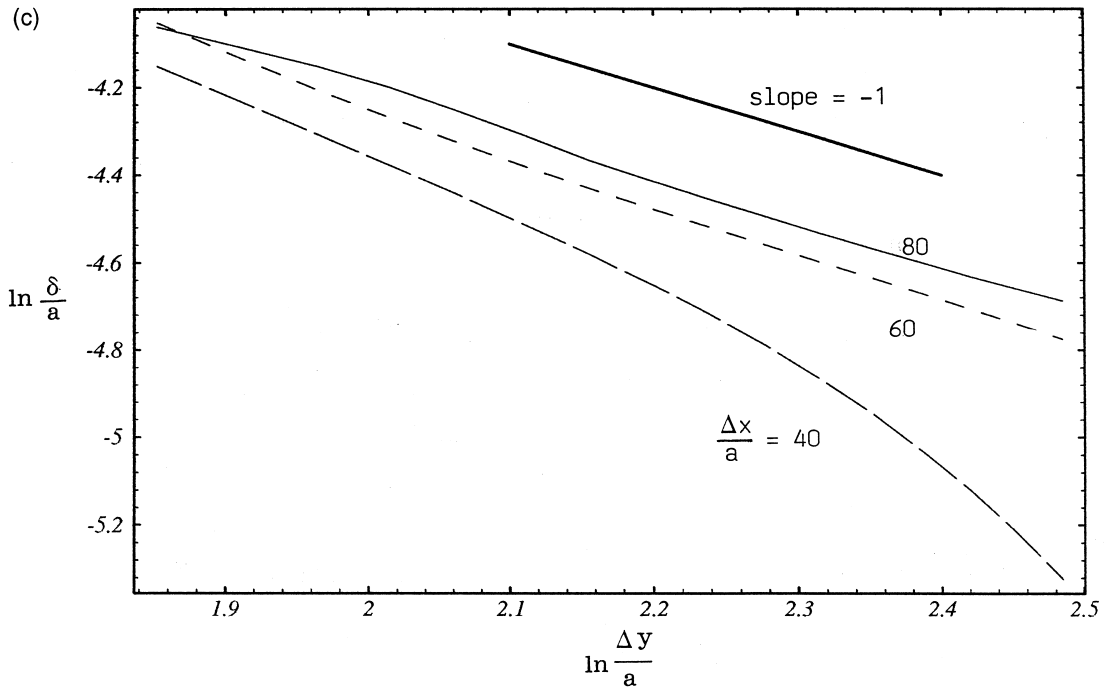

Fig. 2 (*continued*)

Note that the self-diffusivity of deformable particles, such as that of the liquid drops presently considered, is a linear function of the particle number density, whereas the self-diffusivity of perfect disks or spheres is a quadratic function of the particle number density. In the case of disks or spheres, a non-zero net displacement after interception occurs only when a test particle interacts with a particle doublet (Wang et al., 1996).

Unfortunately, because $\delta(\Delta y)$ decays like Δy^{-1}, the integral on the right-hand side of Eq. (4) is not convergent. In physical terms, the divergence of the integral may be attributed to the ill-posedness of two-dimensional infinite Stokes flow: at a distance that is comparable to $a/Re^{1/2}$, where Re is the particle Reynolds number, inertial effects weaken the intensity of the pairwise drop interaction, and $\delta(\Delta y)$ decays at a faster rate. Thus, the self-diffusivity integral is expected to be finite at any nonzero Reynolds numbers, however small. Such difficulties do not arise in three-dimensional Stokes flow where δ decays like $1/(\Delta y^2 + \Delta z^2)$; Δz is the initial separation in the direction of the vorticity of the simple shear flow, and the integral is computed over an infinite plane with respect to the elemental surface area $\mathrm{d}\Delta y\, \mathrm{d}\Delta z$ (Loewenberg and Hinch, 1997). Even in that case, however, inertial effects modify the far-field contribution associated with the interception of widely separated drops, and the integral may be expressed in terms of a regular perturbation expansion with respect to the Reynolds number.

Assuming now that the self-diffusivity integral has been made to converge by including fluid inertia, we proceed to derive an expression for the particle number density flux in the presence of a small number-density gradient. Consider a monodisperse suspension of particles where some of the particles have been tagged. Adopting the formalism of da Cunha and Hinch

(1996), we consider a particular elevation y, a test *tagged* particle located at y' below y, another tagged or untagged particle located at y'' intercepting the test particle, and introduce their initial separation $\Delta y' = y' - y''$. Next, we consider all test particles that undergo the same net displacement $\delta(\Delta y')$, and note that, of them, only those particles that are located within the window $(y - \delta(\Delta y'), y)$ will cross the y level from below. Taking into account that the rate of interception of the test particle with an intercepting particle is given, to leading order, by $G|\Delta y'|$, we find that the upward flux from below is given by

$$j_y^{\mathrm{T,\ Below}}(y) = G \int_0^\infty \left[\int_{y-\delta(\Delta y')}^{y} n^{\mathrm{T}}(y') n(y' - \Delta y') |\, \mathrm{d}\Delta y' |\, \mathrm{d}y' \right] \mathrm{d}\Delta y' \tag{5}$$

where n^{T} is the number density of the tagged particles. We can derive a similar expression for the downward flux from above, and subtract it from that given in Eq. (5) to find the total flux

$$j_y^{\mathrm{T}}(y) = G \int_{-\infty}^\infty \left[\int_{y-\delta(\Delta y')}^{y} n^{\mathrm{T}}(y') n(y' - \Delta y') |\, \mathrm{d}\Delta y' |\, \mathrm{d}y' \right] \mathrm{d}\Delta y' \tag{6}$$

Assuming now that n and n^{T} are only slightly non-uniform, we expand them within the integral on the right-hand side of (6) in Taylor series about y, retain only the constant and linear terms, integrate once, and simplify the resulting expression to obtain the linearized form

$$j_y^{\mathrm{T}}(y) = -D^{\mathrm{s}}(y) \left(\frac{\partial n^{\mathrm{T}}}{\partial y} \right)(y) - n^{\mathrm{T}}(y) \left(\frac{\partial D^{\mathrm{s}}}{\partial y} \right)(y) - G\, n^{\mathrm{T}}(y) \left(\frac{\partial n}{\partial y} \right)(y) \left[\int_{-\infty}^\infty \delta(\Delta y') \Delta y' |\, \mathrm{d}\Delta y' |\, \mathrm{d}\Delta y' \right] \tag{7}$$

or

$$j_y^{\mathrm{T}}(y) = n^{\mathrm{T}}(y)\ V_{\mathrm{p}}^{\mathrm{D}}(y) - \left(\frac{\partial (D^{\mathrm{s}} n^{\mathrm{T}})}{\partial y} \right)(y) \tag{8}$$

where the self-diffusivity is D^{s} is given by Eq. (4). Following the terminology of van Kampen (1981), p. 209, we have introduced the particle drift velocity

$$V_{\mathrm{p}}^{\mathrm{D}} = -\left(\frac{\partial n}{\partial y} \right)(y)\ G \int_{-\infty}^\infty \delta(\Delta y') \Delta y' |\, \mathrm{d}\Delta y' |\, \mathrm{d}\Delta y' \tag{9}$$

The preceding two expressions are consistent with more general expressions presented by Koch (1989) in the limit of small gradients. When the number density n is uniform, we find the familiar Fickian flux $j_y^{\mathrm{T}}(y) = -D^{\mathrm{s}}(\partial n^{\mathrm{T}}/\partial y)(y)$.

When all drops are tagged, we identify n^{T} with n and combine the three terms in Eq. (7) to obtain

$$j_y(y) = -\left(\frac{\partial n}{\partial y} \right)(y) \left\{ n(y) \int_{-\infty}^\infty \delta(\Delta y') \left[\delta(\Delta y') + \Delta y' \right] |\, \mathrm{d}\Delta y' |\, \mathrm{d}\Delta y' \right\} \tag{10}$$

The term in the angular brackets is identified with the gradient diffusivity in a slightly inhomogeneous suspension.

It is instructive to rederive Eq. (10) working within an Eulerian framework, following Wang et al. (1998). We begin by setting

$$j_y(y) = n(y)V_{\mathrm{P}}^{\mathrm{E}}(y) \tag{11}$$

where $V_{\mathrm{P}}^{\mathrm{E}}(y)$ is the Eulerian average drop center velocity, defined as the average velocity of the centers of all drops that cross the elevation y, integrated over the time necessary for a complete interception leading to crossing. The factor $n(y)$ on the right-hand side of Eq. (11) will be divided out in a forthcoming expression defining $V_{\mathrm{P}}^{\mathrm{E}}(y)$. To compute the average drop velocity, we note that a test drop executes a one-parameter family of trajectories depending on its distance from another intercepting drop, and then group the test drops according to these trajectories. If, at a particular time instant t', a drop center is located at y, then the position of a drop before interception was

$$y^{-\infty} = y - \int_{-\infty}^{t'} V(\tau)\,\mathrm{d}\tau \tag{12}$$

where V is the y velocity of the drop center along its path. Integrating over the infinite time of interception, and averaging over all paths, we obtain

$$V_{\mathrm{P}}^{\mathrm{E}}(y) = \frac{G}{n(y)} \int_{-\infty}^{\infty}\int_{-\infty}^{\infty} n\left(y^{-\infty}\right)n\left(y^{-\infty} - \Delta y'\right)|\,\mathrm{d}\Delta y'|V(t')\,\mathrm{d}\Delta y'\,\mathrm{d}t' \tag{13}$$

Assuming now that the drop number density n is only slightly non-uniform, we expand it in two places within the integral in a Taylor series about y, retain only the constant and linear terms, and use Eq. (12) to derive the linearized form

$$V_{\mathrm{P}}^{\mathrm{E}}(y) = G\int_{-\infty}^{\infty}\int_{-\infty}^{\infty}\left\{n(y) - \left(\frac{\partial n}{\partial y}\right)(y)\left[\Delta y' + 2\int_{-\infty}^{t'} V(\tau)\,\mathrm{d}\tau\right]\right\}|\,\mathrm{d}\Delta y'|V(t')\,\mathrm{d}\Delta y'\,\mathrm{d}t' \tag{14}$$

We note that the integral of the first term involving the term $n(y)$ vanishes because the integrand is antisymmetric, compute

$$\int_{-\infty}^{\infty}\int_{-\infty}^{t'} V(\tau)\,\mathrm{d}\tau\; V(t')\,\mathrm{d}t' = \frac{1}{2}\delta^2\left(\Delta y'\right) \tag{15}$$

and substitute the result into Eq. (14) to obtain the right-hand side of Eq. (10).

The slow decay of $\delta(\Delta y)$ undermines the convergence of the integrals on the right-hand sides of Eqs. (9) and (10). Similar convergence difficulties are encountered in the case three-dimensional drops, but not in the case of suspensions of rough spheres where the net displacement after interception is a rapidly decaying function of the initial separation (da Cunha and Hinch, 1996). To suppress the singular behavior, we may perform renormalization following Batchelor (1972) and Wang et al. (1998). First, we may demand that the total areal flux across any y level vanishes, thereby requiring that the fluid move against a transversely

displaced particle, and effectively reducing its net displacement after interception. Mathematically, we replace the particle displacement $\delta(\Delta y)$ by the difference $\delta(\Delta y) - \delta^*(\Delta y)$ at every place on the right-hand side of Eq. (7), where δ^* is the net lateral displacement of a *fluid* point particle after it has intercepted a *single* drop. At large distances Δy, the difference $\delta - \delta^*$ decays at the rate Δy^{-2}. A second renormalization may be effected by requiring that a macroscopic pressure gradient is not established. Unfortunately, even after the dual renormalization, the divergence of the integrals still remains and taking into consideration the fluid inertia appears necessary.

2.4. Flux in wall-bounded flow

In the presence of an infinite plane wall, the velocity at the location of one drop induced by another drop that travels far above the wall decays like Δy^{-2}. To show this, we recall that the velocity due to a point force-diple above a wall decays like Δy^{-2}, and then note that the Stokes flow Green's function remains unchanged when we switch the observation point and the pole and transpose the indices (Pozrikidis, 1992). The faster decay facilitates the convergence of the integrals, but the asymmetry of the particle distribution on either side of a drop leads to a drift velocity due to pairwise interactions, and this must be taken into account when computing the self-diffusivity. An added difficulty is that, close the wall, the net displacement $\delta(y, y')$ is a strong function of the reduced distance of the test drop from the wall, y/a, and the notion of a space-dependent self-diffusivity due to random walks is ill-defined: a drop cannot experience a large number of interceptions while remaining in a virtually unchanged environment.

These concerns, however, do not prevent us from deriving an expression for the flux of the particle number density $j_y(y)$, averaging by ensembles. First, we decompose the flux $j_y(y)$ into a contribution due to the wall $j_y^{\infty}(y)$ given in Eq. (2), and a contribution due to pairwise interactions $j_y^{\text{Pair}}(y)$, as

$$j_y(y) = j_y^{\infty}(y) + j_y^{\text{Pair}}(y) \tag{16}$$

Unfortunately, we are no longer able to use the methods of Section 2.2 to compute the second component $j_y^{\text{Pair}}(y)$, as we cannot arrange the drops in groups exhibiting similar trajectories. This is because the net displacement of a drop after interception depends on the *absolute* lateral positions, as opposed to the *relative* position of the two intercepting drops. The most general expression that we can write for the particle flux from below at a certain y level is

$$j_y^{\text{Below}}(y) = \int_{-\infty}^{y} n(y') R^{\text{Below}}(y', y - y')\, \mathrm{d}y' \tag{17}$$

where $R^{\text{Below}}(y', y - y')$ is the rate of interception of a test drop located at y' with another drop located at y'', subject to the condition that the interception causes the test drop to exhibit a net displacement that is greater than $y - y'$. This expression may be recast into the form

$$R^{\text{Below}}(y', y - y') = G \int_{\Omega^{\text{Below}}} n(y'') |y' - y''|\, \mathrm{d}y'' \tag{18}$$

where the domain of integration Ω^{Below} is the support of the function $\delta(s, s')$ for $\delta(s, s') >$

$y - y'$. We can write a similar expression for the flux from above, and subtract it from Eq. (17) to obtain the net flux

$$j_y(y) = \int_{-\infty}^{y} n(y') R^{\text{Below}}(y', y - y')\, \mathrm{d}y' - \int_{y}^{\infty} n(y') R^{\text{Above}}(y', y - y')\, \mathrm{d}y' \tag{19}$$

where $R^{\text{Above}}(y',\ y - y')$ is the rate of interception of a test drop located at y' with another drop located at y'', subject to the condition that the interception causes the test drop to exhibit a net displacement that is less than $y' - y$.

It is reassuring to confirm that Eq. (19) is consistent with the expressions derived earlier for infinite shear flow. Substituting Eq. (18) into (17), and noting that the net displacement after interception decreases monotonically with the initial separation from maximum value $\delta_{\max}$, we find

$$j_y^{\text{Below}}(y) = \int_{y-\delta_{\max}}^{y} \left[\int_{y'-\zeta(y-y')}^{y'} n(y') n(y'') |y' - y''|\, \mathrm{d}y'' \right] \mathrm{d}y'$$

$$= \int_{y-\delta_{\max}}^{y} \int_{0}^{\zeta(y-y')} n(y') n(y' - \chi) |\chi|\, \mathrm{d}y''\, \mathrm{d}y' \tag{20}$$

where $\zeta(y - y')$ is the initial separation that causes a net displacement equal to $\delta = y - y'$. The function $\zeta(\delta)$ is the inverse of the function plotted in Fig. 2(b). Switching the variables of integration in Eq. (23) yields Eq. (5) with n^{T} in place of n.

Assuming that the number density n particles is only slightly non-uniform, we expand it in two places within the integral in Eq. (19) in a Taylor series about y, and retain only the constant and linear terms to obtain the linearized form

$$j_y(y) = n(y) V_{\text{P}}^{\text{D-S}}(y) - D^{\text{G}} \left[\frac{\partial n}{\partial y} \right] (y) \tag{21}$$

where we have introduced the Stratonovich drift velocity

$$V_{\text{P}}^{\text{D-S}}(y) \equiv G\, n(y) \left\{ \int_{-\infty}^{y} \left[\int_{\Omega^{\text{Below}}} |y' - y''|\, \mathrm{d}y'' \right] \mathrm{d}y' - \int_{y}^{\infty} \left[\int_{\Omega^{\text{Above}}} |y' - y''|\, \mathrm{d}y'' \right] \mathrm{d}y' \right\} \tag{22}$$

and the gradient diffusivity

$$D^{\text{G}} \equiv G\, n(y) \left\{ \int_{-\infty}^{y} \left[\int_{\Omega^{\text{Below}}} (2y - y' - y'') |y' - y''|\, \mathrm{d}y'' \right] \mathrm{d}y' \right.$$

$$\left. - \int_{y}^{\infty} \left[\int_{\Omega^{\text{Above}}} (2y - y' - y'') |y' - y''|\, \mathrm{d}y'' \right] \mathrm{d}y' \right\} \tag{23}$$

(van Kampen, 1981, p. 244; Young, 1994). The study of these integrals requires a large amount of computational work and was not attempted.

2.5. Simulations of pairwise interactions in a periodic suspension

To explicitly illustrate the migration of the drops away from a wall and also investigate the direction and magnitude of the net drop displacement after interception, we simulated the motion of a singly-periodic suspension consisting of two infinite arrays of identical drops, each with period L, subject to a simple shear flow with shear rate G, as shown in Fig. 1(b). At the initial instant, the interfaces are circular, and the arrays are placed in a staggered formation, separated along the x-axis by the distance $L/2$. The ratio of the equivalent drop radius, a, to the period of each array, L, was set equal to 0.05. Thus, the initial drop separation along the x-axis is ten times the drop radius, which is long enough for the effect of the periodicity to be unimportant.

The motion of the drops was computed by the method of interfacial dynamics for Stokes flow. To avoid computing the hydrodynamic potentials over the wall, the integral equation for the interfacial velocity was written with respect to the periodic Green's function of Stokes flow in a semi-infinite domain bounded by a plane wall. Closed-form but lengthy expressions for this Green's function and its associated stress tensor in terms of arrays of image singularities are provided by Pozrikidis (1992), and a subroutine that produces them is available from the second author on request. The shape of a drop interface between two successive marker points was approximated with blended circular arcs. When the viscosity ratio is other than unity, the integral equation was solved by the method of successive substitutions.

To discuss the motion of the drops, we introduce the functions $x = x_{ci}(t)$, $y = y_{ci}(t)$, where $i = 1, 2$, describe, respectively, the trajectory of the centroid of the first or second drop. In Fig. 3(a), we display the functions $y_{ci}(t)$ for drops with $\lambda = 1$ at $Ca = 0.294$, for $y_{c1}(t = 0)/L = 0.2$ and $y_{c2}(t = 0)/L = 0.1,\ 0.15,\ 0.25,\ 0.3,\ 0.35$; the capillary number is defined as $Ca = \mu G a/\gamma$. Corresponding drops pairs may be identified by matching line thicknesses. In all cases, we observe continuous migration away from the wall at a rate that is a rapidly decreasing function of the distance from the wall, interrupted by drop interceptions as one periodic array passes over or under the other. The net displacement of the drops in the top array from the solitary path is positive, and that of the drops in the lower array is negative, with one exception: when $y_{c2}(t = 0)/L = 0.15$, at first interception, the drops in the second array become aligned with, and then move higher than, the drops in the first array, only to return below the first array during the second and subsequent interceptions. Thus, in the presence of a wall, two intercepting drops may exhibit a net displacement whose sign is opposite to that of the displacement in infinite shear flow. Since inertia is absent, the overpassing must be attributed to a subtle interaction between the deformed interfaces at close proximity.

The effect is seen more clearly in Fig. 3(b), which is the counterpart of Fig. 3(a) for less deformable drops corresponding to $Ca = 0.1$. As expected, the rate of migration away from the wall at $Ca = 0.10$ is less than at 0.294. The most interesting new feature is the leap-frogging of the drop positions for $y_{c2}(t = 0)/L = 0.15$ during a sequence of three interceptions over the extended period of the simulation shown. The dashed lines in this figure represent the trajectories of a pair of non-periodic drops, included to demonstrate that the periodicity of the flow is not responsible for the switching of the drop vertical positions. The inset in Fig. 3(b) shows drop interface profiles at several times during the flow of a periodic suspension with $y_{c2}(t = 0)/L = 0.15$.

Switching of the relative drop positions during interception occurs for values of the viscosity ratio other than unity, as long as the drop centers are sufficiently close to each other and to the wall. This is seen clearly in Fig. 3(c) which is the counterpart of Fig. 2(a) for $\lambda = 0.10$.

3. Expansion of a suspension bed above a wall

In Section 2, we discussed the motion of a drop in a semi-infinite dilute suspension bounded by a single plane wall, in terms of pairwise drop interceptions. A theory for the motion of a drop in a non-dilute suspension, accounting for multi-drop interactions, is not available, and progress must rely on numerical simulations.

Durlofsky and Brady (1989) simulated the expansion of a bed of neutrally buoyant spherical particles placed next to the lower wall of Couette flow channel, and demonstrated the onset of particle resuspension due to hydrodynamic interactions. We consider the analogous problem of the expansion of a bed of two-dimensional drops subject to an overpassing simple shear flow,

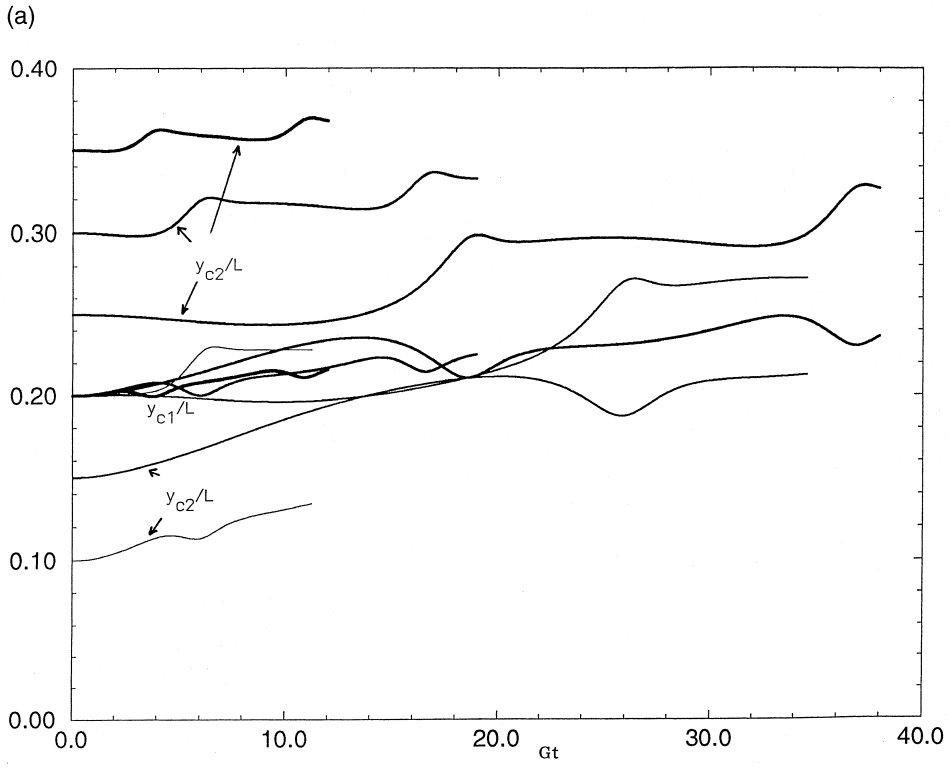

Fig. 3. (a) Evolution of the lateral position of the drop centroids in a periodic suspension consisting of two arrays of drops, for $a/L = 0.05$, $\lambda = 1$, and $Ca = 0.293$. At the initial instant, the interfaces are circular, and the drops are separated by the distance 0.5 L. The initial lateral position of the drops in the first or second array are $y_{c1}(t = 0)/L = 0.2$ and $y_{c2}(t = 0)/L = 0.1$, 0.15, 0.25, 0.3, 0.35. The thickness of the lines increases monotonically with increasing the initial vertical position of the drops in the second array. (b) Same as (a) but for $Ca = 0.10$. The inset shows profiles at times $Gt = 0$, 12, 31, 50. (c) Same as (b) but for $\lambda = 0.1$.

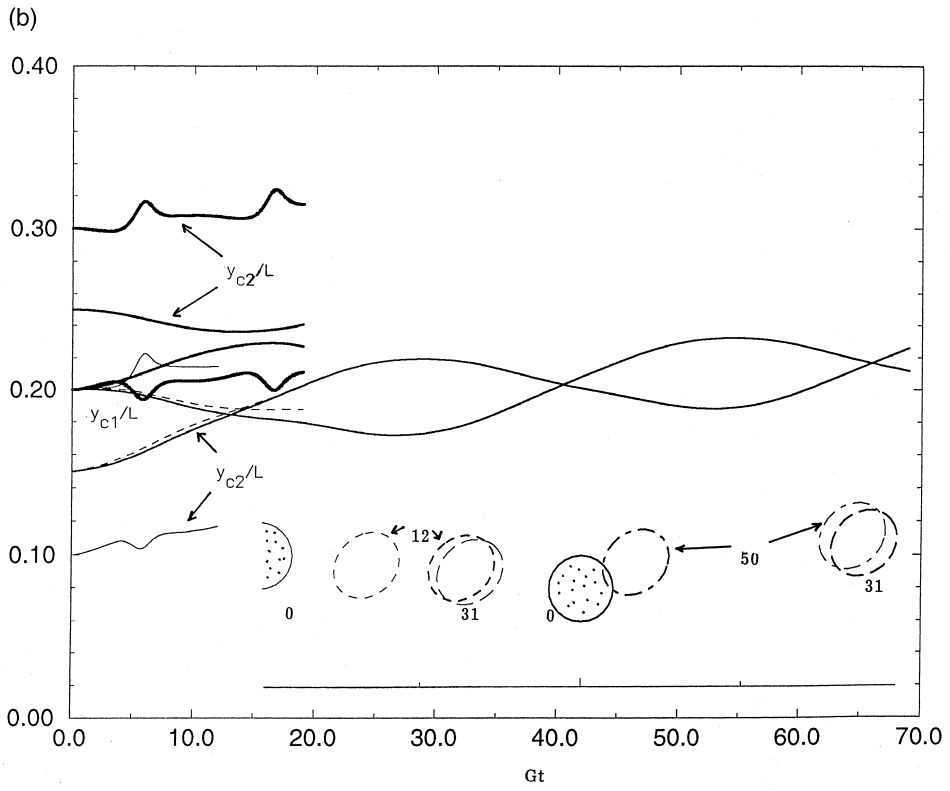

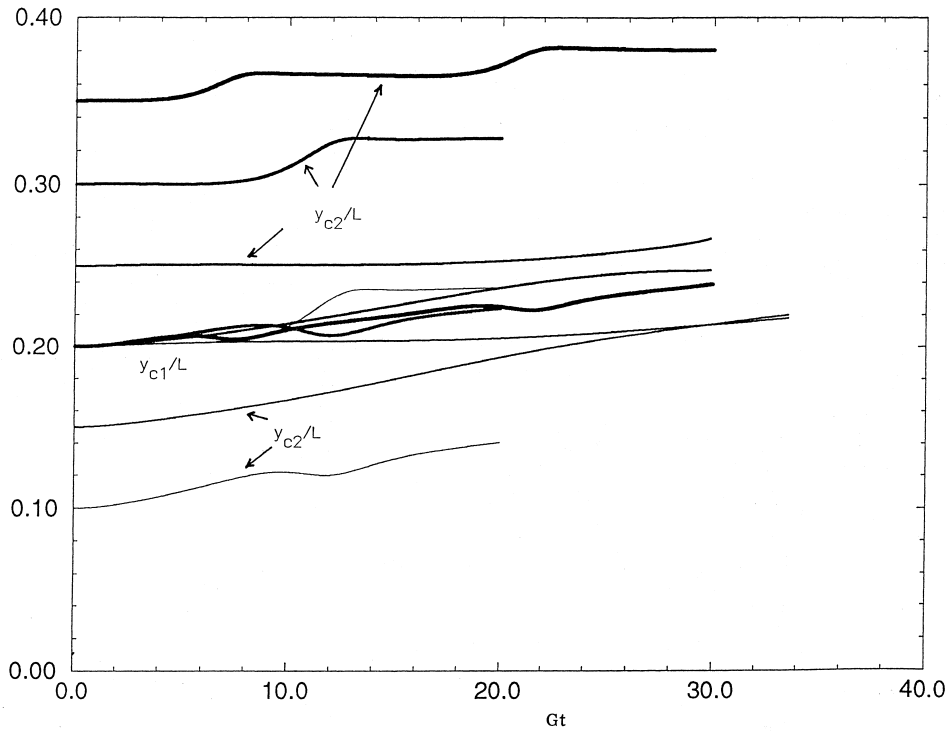

Fig. 3 (*continued*)

as illustrated in Fig. 4(a), with three objectives: (a) to investigate, in quantitative terms, the formation of a particle-free zone near the wall due to drop migration and drop interception, (b) to illustrate how the random motion of the drops smears out the interface and causes the bed to grow, and (c) to estimate the rate of expansion. This hydrodynamic model is analogous, but not identical, to a molecular diffusion model where an initially uniform layer of a species is placed next to a wall, and is then allowed to grow due to diffusion while the no-flux condition is required over the wall. An additional feature of the hydrodynamic model is the presence of a hydrodynamic potential causing the drops the migrate away from the wall.

In the numerical simulations, 25 identical drops were distributed randomly within a square box next to the wall. The drop centers were placed at the nodes of a regular 5×5 square lattice, and were displaced in a random fashion parallel and normal to the wall by distances that are sufficiently small to prevent overlapping. The configuration was then replicated along the wall with period L. The equivalent drop radius a was set equal to 0.05 L, yielding an areal fraction $\phi = 25\pi a^2/L^2 = 0.196$, which is large enough so that the suspension is not dilute, but low enough so that difficulties associated with stiffness of the governing equations do not to arise. The motion of the drops was simulated using the method of interfacial dynamics for Stokes flow discussed in Section 2.

Two simulations were performed with $\lambda = 1$ and $Ca = 0.10$ or 0.294, starting with the same initial configuration; the capillary number was defined in Section 2. Each simulation was carried out up to approximately $Gt = 70$ using the first-order Euler method and a constant time step of $G\,\Delta t = 0.02$, requiring approximately 10 days of CPU time on a SUN SPARCstation 20 for each case. The area of each drop was normalized by isotropic expansion or contraction about its center after each step, so that the areal fraction was kept precisely constant during the simulation. Simulations with $\lambda \neq 1$ were attempted but proved too memory demanding and computationally intensive even on the fastest available computer CRAY T90.

Fig. 4(a)–(c) display typical profiles of the evolving suspension for $\lambda = 1$ and $Ca = 0.294$, at $Gt = 0$, 29.4, 68.4. Cursory inspection reveals several interesting features. First, the drops next to the wall gradually migrate away from the wall and enter the bulk of the bed. Second, there is a well-defined row of drops next to the wall throughout the simulated motion. Initially, this row contains five drops per periodic box, but as the wall-drops intercept other overpassing drops, they are drawn into the bulk of the suspension and then engage in a motion that is typical of that occurring in a homogeneous suspension. Third, the interface between the suspension and the clear fluid above progressively smears out, and the thickness of the bed increases due to occasional excursions of the top drops caused by interceptions. Fourth, Fig. 4(b) and (c) reveal the formation of significant drop agglomerates in the bulk of the bed due to strong interactions.

To discuss the evolution of the bed in quantitative terms, we introduce the dimensionless areal density of the suspension $\omega(y)$, defined such that the integral of $\omega(y)$ with respect to y from 0 to b is equal to the area of the suspended phase confined between the wall and the line $y = b$, per period of the suspension. The integral of $\omega(y)$ with respect to y from 0 to ∞ is thus equal to the total area of the suspended phase per period. To expedite the computation of $\omega(y)$, we approximate the drop interfaces with circles centered at the instantaneous drop centroids, and then compute $\omega(y)$ using analytical expressions. In Fig. 4(d), we present graphs of $\omega(y/L)$ at $Gt = 0$ and 68.4, shown with circles or squares. In spite of the significant

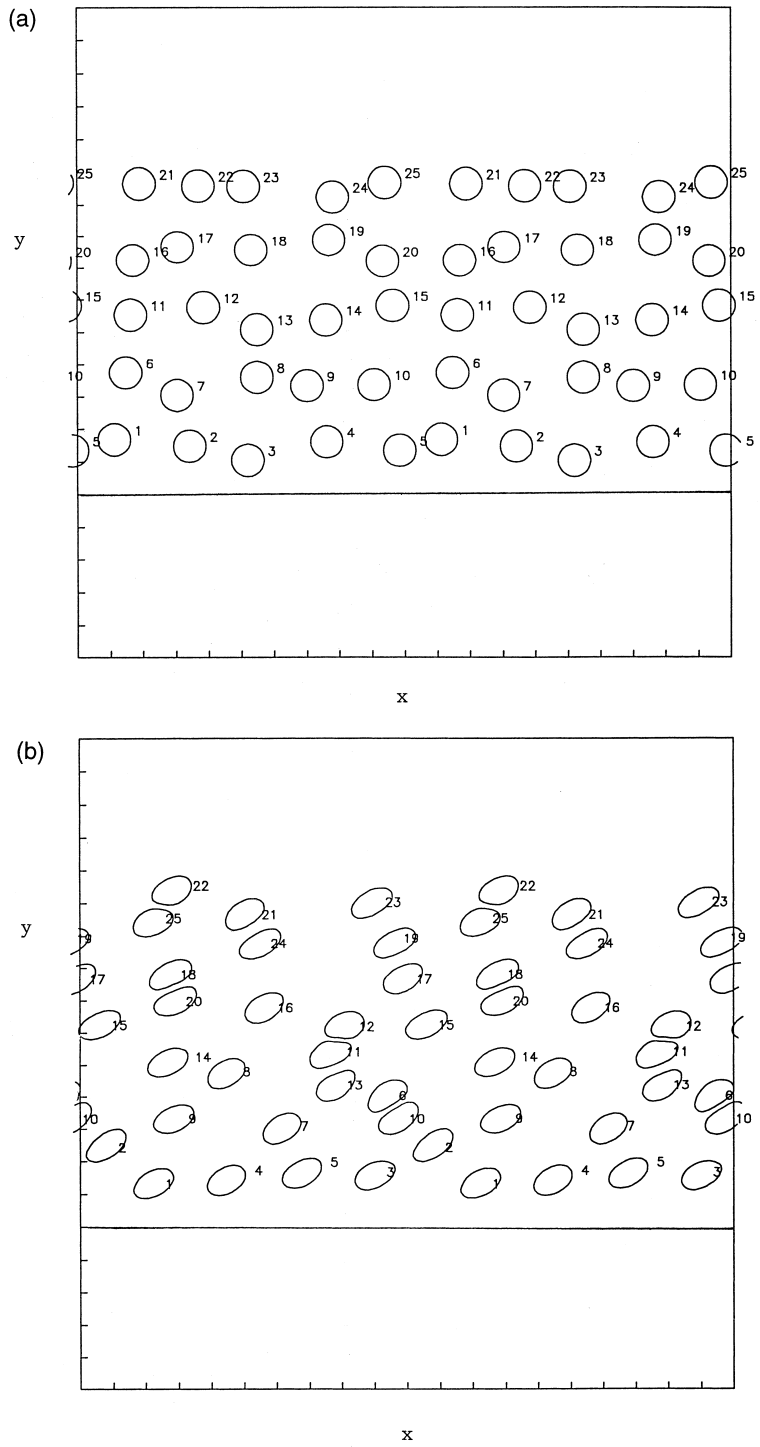

Fig. 4. (a–c) Stages in the expansion of a periodic bed containing 25 drops per periodic box, for $\lambda = 1$, $Ca = 0.294$, at times $Gt = 0$, 29.4, 68.4. (d) Graphs of the areal density of the suspension $\omega(y)$ at $Gt = 0$ (circles) and 68.4 (squares). (e) Evolution of the mean lateral drop centroid position $\langle y_c \rangle$ marked as (i), variance $\langle y_c^2 \rangle$ marked as (ii), variance $\langle (y_c - \langle y_c \rangle)^2 \rangle$ marked as (iii), and $d^2 = [\max(y_c) - \max(y_c(t = 0))]^2$ marked as (iv).

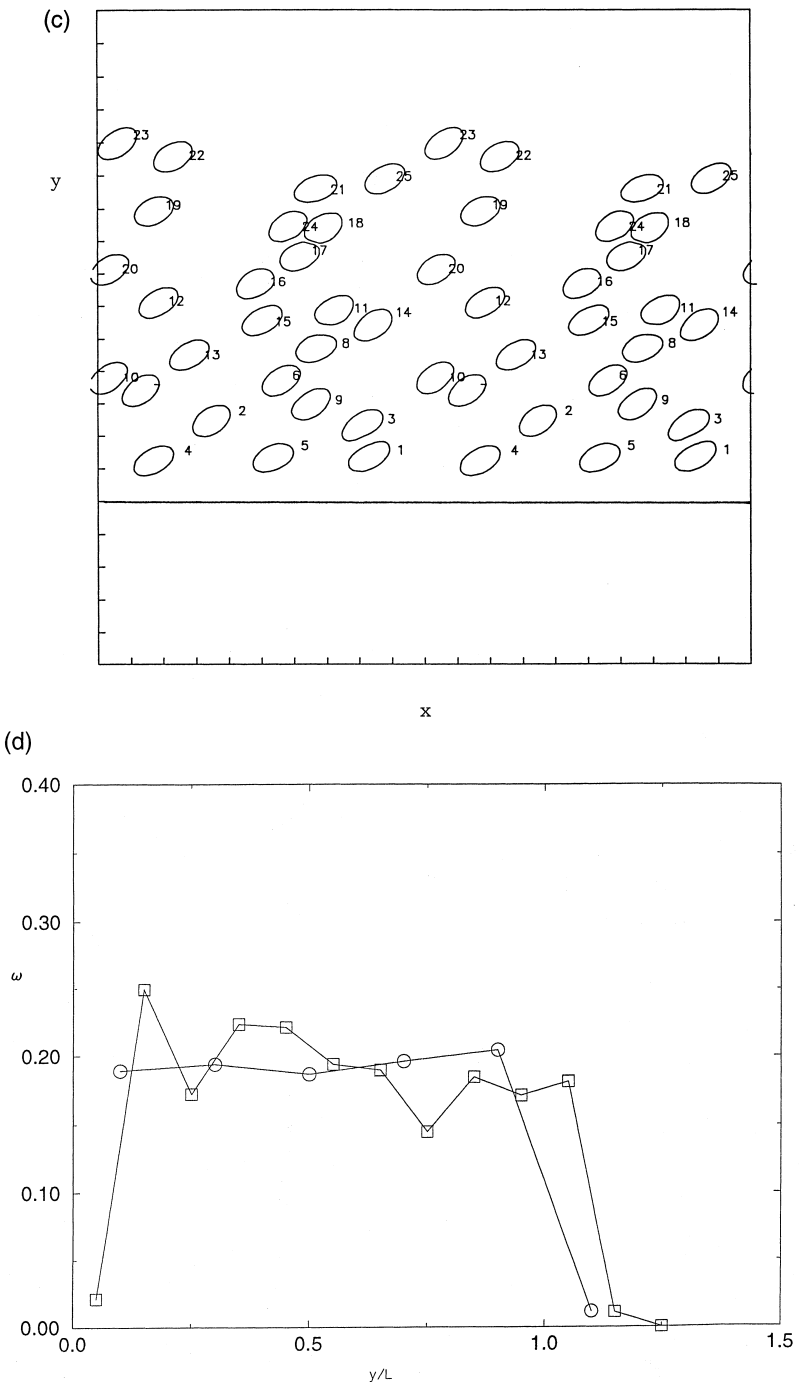

Fig. 4 (*continued*)

numerical noise due to the small size of the simulated system, the formation of a drop-free zone next to the wall and the expansion of the bed are apparent. The drops next to the wall move away from the wall due to spontaneous migration, and toward the wall due to hydrodynamic dispersion mediated by interceptions with other drops in the main body of the bed. This observation suggests that, at long times, the thickness of the particle-free wall zone will tend to an equilibrium value where the migration flux balance the diffusion flux due to interceptions. If the drops were heavy, the motion due to gravity would also contribute to this balance.

Further quantitative information on the expansion of the bed can be gained by examining the history of the mean drop centroid lateral position $\langle y_c \rangle$, variances $\langle y_c^2 \rangle$, $\langle (y_c - \langle y_c \rangle)^2 \rangle$, and positive measure $d^2 = [\max(y_c) - \max(y_c(t=0))]^2$, all expressing the thickness of growing bed. The pointed brackets indicate average over all drops in a periodic box. Fig. 4(e) displays the evolution of these diagnostics showing an initial adjustment period lasting up to $Gt = 20$, and then a period of nearly linear growth with slopes of same order of magnitude. The slope $\mathrm{d}\langle y_c^2 \rangle / \mathrm{d}t$ in the linear regime, corresponding the line marked ii, is approximately equal to $0.00045\, G\, L^2 = 0.175\, G\, a^2$, which is one order of magnitude higher than the self-diffusivity of a drop in a homogeneous suspension at the areal fraction $\phi = 0.196$ for $Ca = 0.294$ (Li et al., 1996). It is tempting to compare the evolution of the drop number density distribution with that predicted by a similarity solution of the unsteady diffusion equation showing that the variance grows in time as like $t^{2/3}$. In the case of drops, however, dispersion relies on hydrodynamic interactions, and the effective diffusivity is a strong function of the local drop number density.

Similar results were obtained for the lower capillary number $Ca = 0.1$, with quantitative differences observed due to the lower drop deformability. Fig. 5(a) displays instantaneous drop

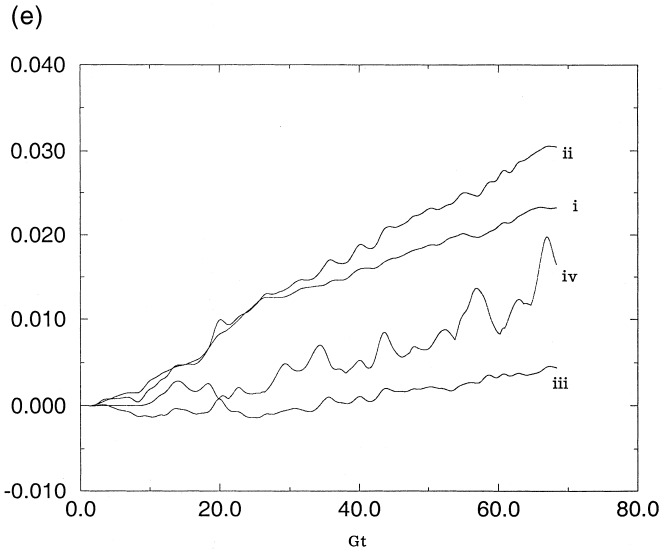

Fig. 4 (*continued*)

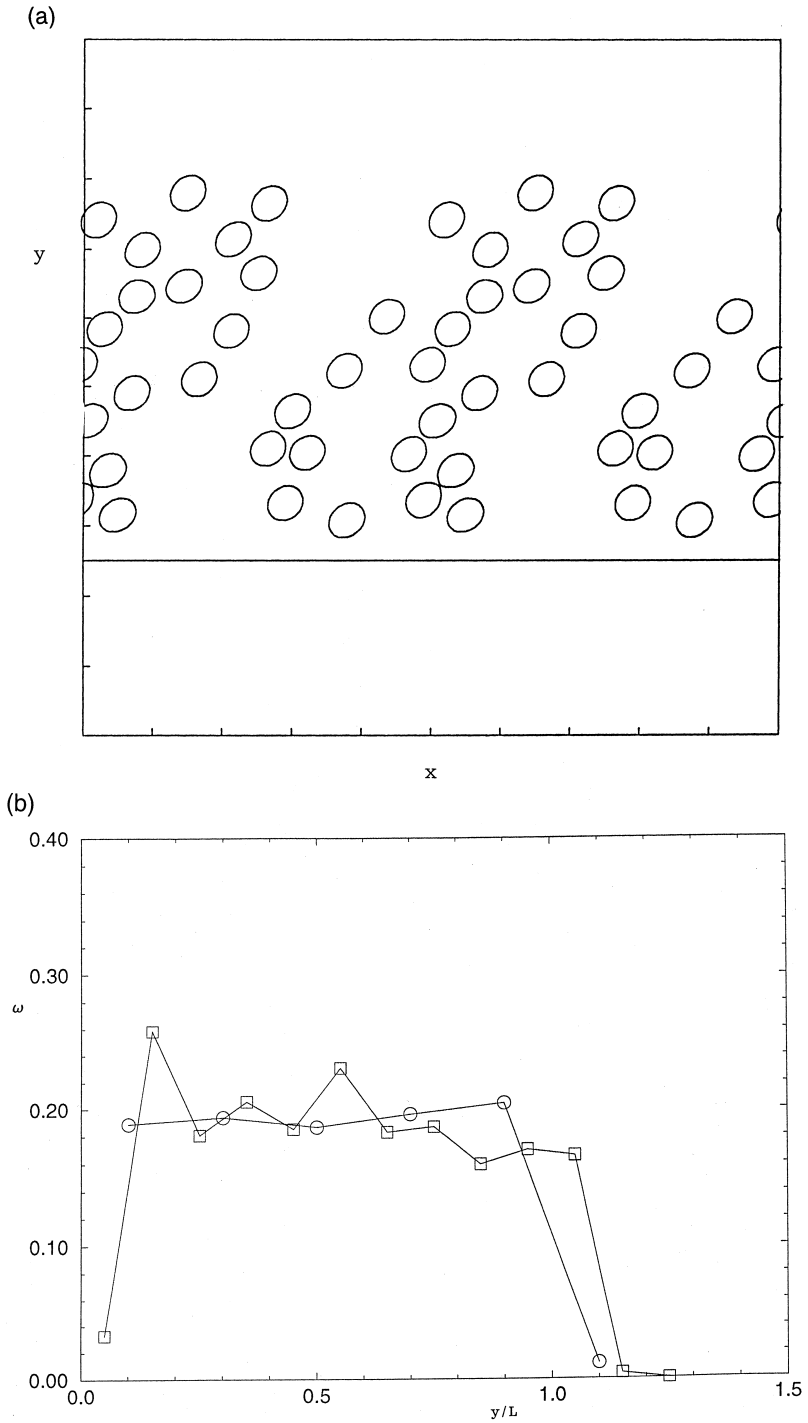

Fig. 5. (a) A typical stage in the expansion of a periodic bed containing 25 drops per periodic box, for $\lambda = 1$, $Ca = 0.10$, at $Gt = 62.4$. (b) Graphs of the areal density of the suspension $\omega(y)$ at $Gt = 0$ (circles) and 62.4 (squares). (c) Evolution of the mean lateral drop centroid position $\langle y_c \rangle$ marked as (i), variance $\langle y_c^2 \rangle$ marked as (ii), variance $\langle (y_c - \langle y_c \rangle)^2 \rangle$ marked as (iii), and $d^2 = [\max(y_c) - \max(y_c(t = 0))]^2$ marked as (iv).

profiles of the expanded bed at $Gt = 62.4$; the initial profile is identical to that displayed in the Fig. 4(a). At this low capillary number, the drops are only slightly deformed. Fig. 5(b) displays the areal density of the suspension $\omega(y)$ at $Gt = 0,62.4$, and Fig. 5(c) displays the history of the mean lateral drop center position $\langle y_c \rangle$, variances $\langle y_c^2 \rangle$, $\langle (y_c - \langle y_c \rangle)^2 \rangle$, and d^2. The slopes of these graphs in the linear growth regime are significantly lower than the corresponding ones for $Ca = 0.294$, and this underlines once more the importance of the deformability of the drops.

4. Pressure-driven channel flow

In the Section 3, we investigated the effect of a wall on the lateral motion of drops in a suspension undergoing simple shear flow. The numerical simulations illustrated the formation of a drop-free zone next to the wall due to spontaneous migration, and the dispersion of the drops due to hydrodynamic interactions. These results are relevant to the local dynamics of a suspension when the length scale of the unperturbed flow is large compared to the drop size, so that its spatial variation and the associated local pressure gradient are not important. In this section, we consider the motion when the last condition is not met; that is, we consider the unidirectional flow of a suspension with the position-dependent shear rate due to a pressure gradient. In this case, in addition to the aforementioned two types of motion, there is a third type of motion due to the curvature of the velocity profile whose significance we wish to investigate.

Zhou and Pozrikidis (1994) studied the pressure-driven flow of a non-dilute monodisperse periodic suspension of two-dimensional liquid drops in a channel that is bounded by two parallel walls, as depicted in Fig. 6. In their numerical simulations, they computed the motion

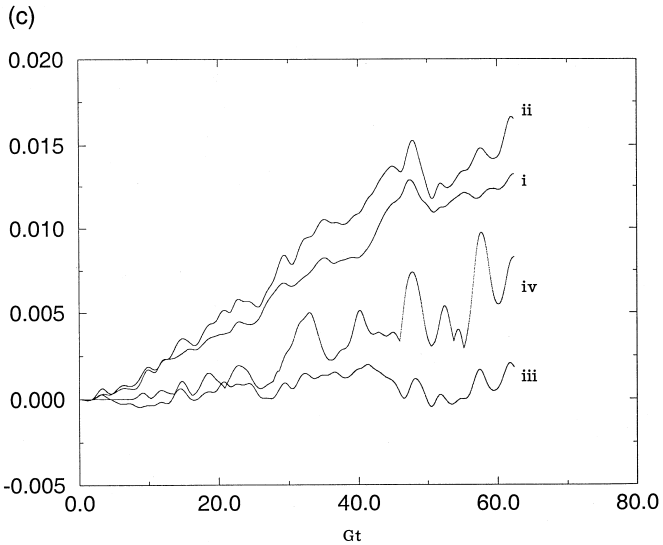

Fig. 5 (*continued*)

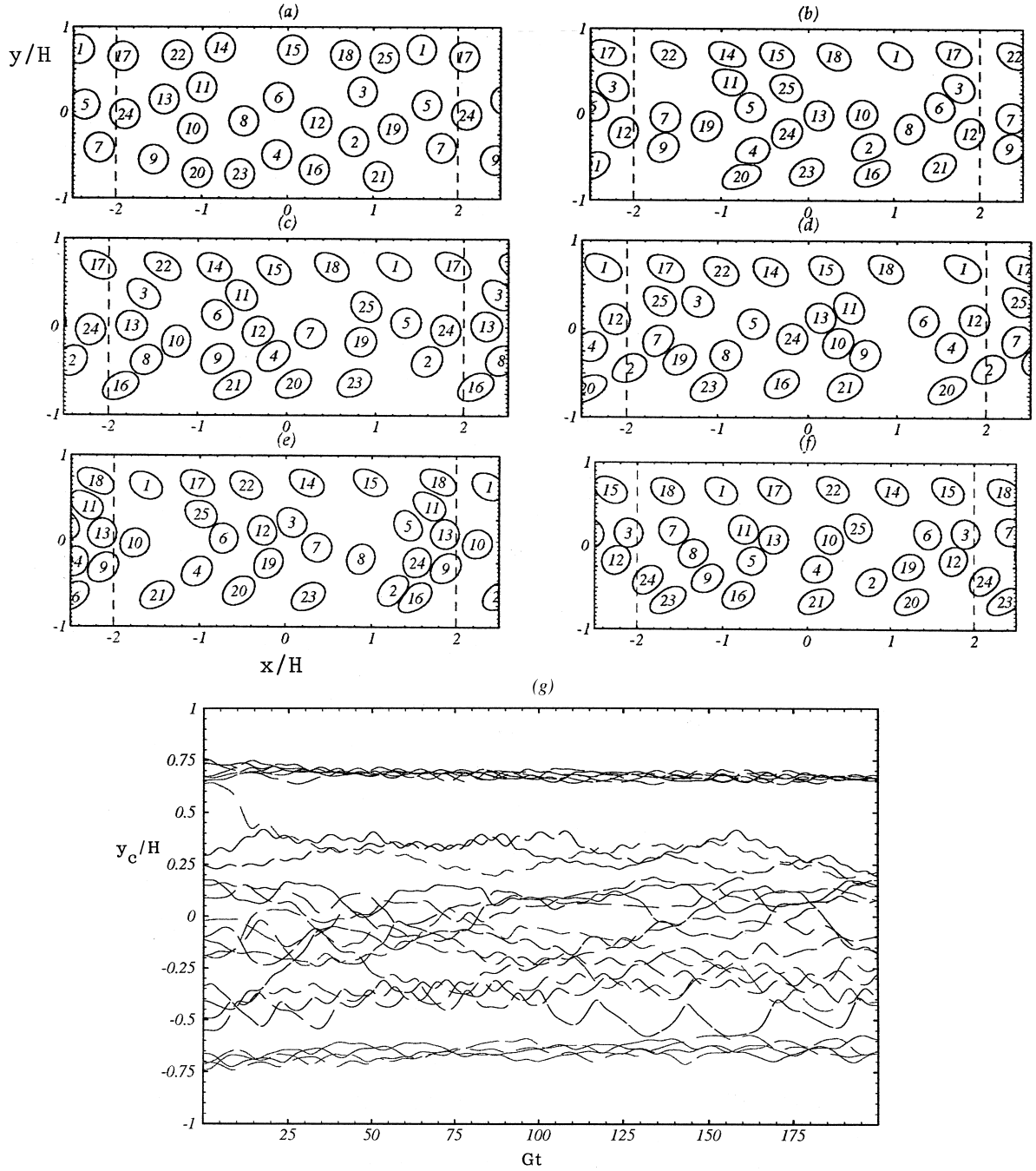

Fig. 6. Simulation of the motion of a suspension of two-dimensional liquid drops in a channel bounded by two parallel walls, for $\lambda = 1$, $Ca = 0.1732$. (a–f) Instantaneous drop profiles at dimensionless times $\hat{t} = 0$, 40, 80, 120, 160, 200. (g) Evolution of the lateral position of the drop centroids. (h, i) Drop number density distribution and velocity profile averaged over the simulation time after equilibration. (j) The solid line shows the evolution of the relative effective viscosity of the suspension, and the dashed lines shows the mean deformation of the drops averaged over all drops.

of 12 drops suspended with each period of the flow for viscosity ratio $\lambda = 1$, and found that randomly distributed drops settle into ordered arrays that exhibit stable motion. We presently extend the earlier results to a larger system of 25 drops per periodic box, and to values of λ larger than unity. The extension to a higher number of drops allows us to study certain aspects of the statistics of the evolving configuration.

The numerical method is similar to that described by Zhou and Pozrikidis (1994), with some improvements. Each drop interface is described by a set of marker points, and the Cartesian coordinates of points along the interface are approximated using cubic-spline interpolation with respect to the arc length of the polyline connecting the marker points. The accuracy of the approximation is improved by re-interpolating using these first-generation cubic splines. For $\lambda = 1$, points are inserted or removed in the course of the simulation to resolve regions of high curvature and prevent clustering. The time integration is carried out by the second-order Runge-Kutta method. For $\lambda \neq 1$, considerations of computational cost restrict the number of marker points along each interface to the highest affordable value of 32. In this cases, the marker points are redistributed evenly with respect to arc length after each time step, and the time integration is carried out by the explicit Euler method. Keeping the maker points equidistant significantly improves the rate of convergence of the iterative method used to solve the integral equation, and thereby minimizes the run times.

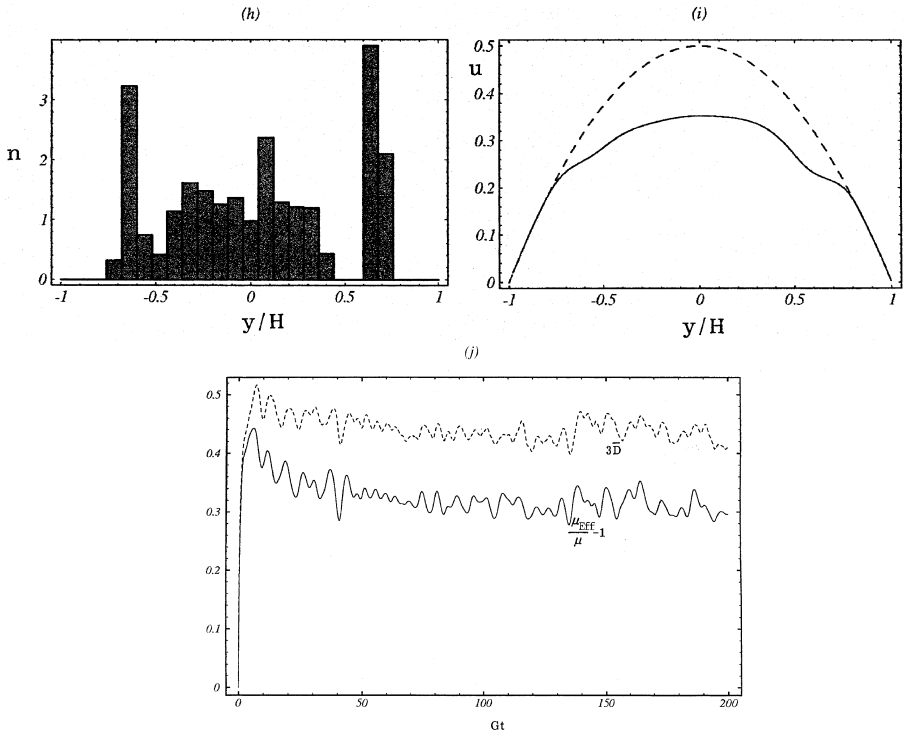

Fig. 6 (*continued*)

The simulations have become feasible thanks to the implementation of an efficient method for computing the periodic Green's function of Stokes flow in a channel that is bounded by parallel walls. The method is based on trilinear interpolation of the non-singular components of the Green's function through look-up tables. The interpolation is done with respect to (a) the difference in the x coordinates, and (b) the y coordinates of the observation point and the pole. The dimension of the interpolation grid is 129^3, yielding an absolute error on the order of 10^{-4} for each Green's function evaluation. The interpolation code was fully vectorized on the CRAY T90 of the San Diego Supercomputer Center. Vectorization reduces the CPU time almost by a factor of 100.

In the simulations, the length of the periodic computational domain L was set equal to twice the clearance of the channel $2H$, $L = 4H$, to yield a rectangular computational domain, and the areal fraction of the drops was fixed at the value $\phi = 0.2945$. Accordingly, the ratio of the equivalent drop radius a to the channel semi-width H is $a/H = 0.1731$. The initial distribution of the drop centers, shown in Fig. 6(a), was determined by a random-number generator with care taken to prevent overlap, and was kept the same in all simulations. A simulation up to reduced time $\hat{t} \equiv t\,\beta H/\mu = 200$ on the CRAY T90 requires 11 h of CPU time for $\lambda = 1$, and 23 h for $\lambda \neq 1$; β is the negative of the axial mean pressure gradient, and μ is the viscosity of the suspending fluid.

Fig. 6(a)–(f) show typical stages in the evolution of a suspension for fluids with equal viscosity, $\lambda = 1$, and capillary number $Ca \equiv \beta H a/2\gamma = 0.1732$, where γ is the interfacial tension, at reduced times $\hat{t} = 0$, 40, 80, 120, 160, 200. One interesting, but not unexpected, feature of the motion is the reduced deformation of the drops near the centerline of the channel compared with the deformation of the drops near the channel walls, as a result of the reduced shear rate near the centerline. Fig. 6(g) displays the evolution of the lateral position of the drop centroids showing the migration of drops away from the walls at a rate that decreases monotonically in time during the simulation. There is one well-defined layer of drops next to each wall; the top one consisting of drops 1, 17, 22, 14, 15, and 18, and the bottom one consisting of drops 21, 20, 23, 16. The rest of the drops are engaged in a seemingly disorganized motion.

The behavior described in the preceding paragraph is in stark contrast with that reported by Zhou and Pozrikidis (1994) for a system of 12 drops per period, where a three-row formation was observed to develop regardless of the initial arrangement. It appears that for a fixed volume fraction, there is a critical number of drops per periodic box where the character of the motion changes from organized to random; for the conditions presently considered, this number lies somewhere between 12 and 25. If the suspension were not periodic, there would be a critical value of the ratio a/H above which the drop would arrange themselves in rows and below which they would engaged in random motion. The transition from one type of behavior to the other occurs, presumably, through a hydrodynamic instability. The physical relevance of these results is corroborated by the recent observations of Hampton et al. (1997) who reported spontaneous formation of particle layers in tube flow at sufficiently large volume fractions and particle diameters.

Fig. 6(h) displays the drop center number density distribution averaged with respect to dimensionless time $\hat{t}$ over the interval (90, 200). In spite of the significant noise, two features are clear: the number density distribution over the central region of the channel is flat, and a

"double- humped" distribution is apparent. The notable peaks near the walls reflect the aforementioned presence of two rows of drops next to the walls. Double-humped distributions of concentration profiles in tube flow were reported by Kowalewski (1984), Fig. 5), along with the observation that the wall maximum for low viscosity drops decreases with downstream position due to drop migration away from the walls. Hiller and Kowalewski (1987) report that for $\lambda = 1$, the wall peak rises with downstream position and then moves slowly toward the centerline. Weak maxima near a tube wall were also reported by Hampton et al. (1997) for suspensions of rigid particles, over a broad range of volume fractions.

Nott and Brady (1994) simulated the pressure-driven flow of a suspension of spherical particles between two parallel plates, and found that the particles tend to accumulate at the channel centerline where the number density distribution is blunt but not as flat as that shown in Fig. 6(h). This comparison appears to suggest that deformable liquid drops are distributed in a channel more uniformly than solid particles, in spite of their natural tendency to migrate away from the walls. Strong lubrication forces developing between intercepting solid particles appear to play a key role in keeping the particles away from the walls. The experiments of Hampton et al. (1997) corroborate the result of this comparison, although the significant noise in the data shown in Fig. 6(h) does not allow for definitive conclusions.

Fig. 6(i) depicts the mean fluid velocity profile computed by averaging the pointwise velocity over several x position within a period, and then averaging over time after equilibration; this doubly averaged velocity would be measured in the laboratory by a non-intrusive velocity probe. The dashed line indicates the unperturbed parabolic profile of the Hagen-Poiseuille flow. The most interesting feature is the wide region of near plug-flow, extending over 3/10 the clearance of the channel. A comparison with the results of Nott and Brady (1994) shows that the blunting of the velocity profile is less prominent for viscous drops than for solid particles, in agreement with the observations of Kowalewski (1980).

Fig. 6(j) displays the evolution of the suspension effective viscosity computed in terms of the axial flow rate, as discussed by Zhou and Pozrikidis (1994), and the average instantaneous deformation of all drops $\langle D \rangle$. As the drops start deforming, the relative effective viscosity μ_{Eff}/μ rises from the value of unity, reaches a maximum, and settles to the equilibrium value of 1.3 around which it fluctuates. The dimensionless equilibration time is approximately equal to $\hat{t}_{\text{Eq}} = 90$. The overshooting of the effective viscosity during the initial relaxation period is attributed to an initial adjustment and subsequent migration of the drops toward the centerline. The average deformation of the drops shows a similar behavior. It is interesting to note that peaks and valleys of the effective viscosity show excellent correlation with peaks and valleys in the average deformation, and this confirms the intimate relation between the instantaneous geometry of the interfaces and the rheological properties of the suspension observed in previous studies of homogeneous flow.

The equilibration time t_{Eq} may be used to define an effective suspension diffusivity for channel flow, $D_{\text{Eff}} \equiv a^2/t_{\text{Eq}}$; in dimensionless form, $\hat{D}_{\text{Eff}} \equiv D_{\text{Eff}}\mu/(\beta H a^2) = 1/\hat{t}_{\text{Eq}} = 0.0111$, which is on the order of $(a/H)^2 = 0.0300$. This observation suggests the scaling

$$\hat{D}_{\text{Eff}} \cong F(\phi, Ca, \lambda)\left(\frac{a}{H}\right)^2 \tag{24}$$

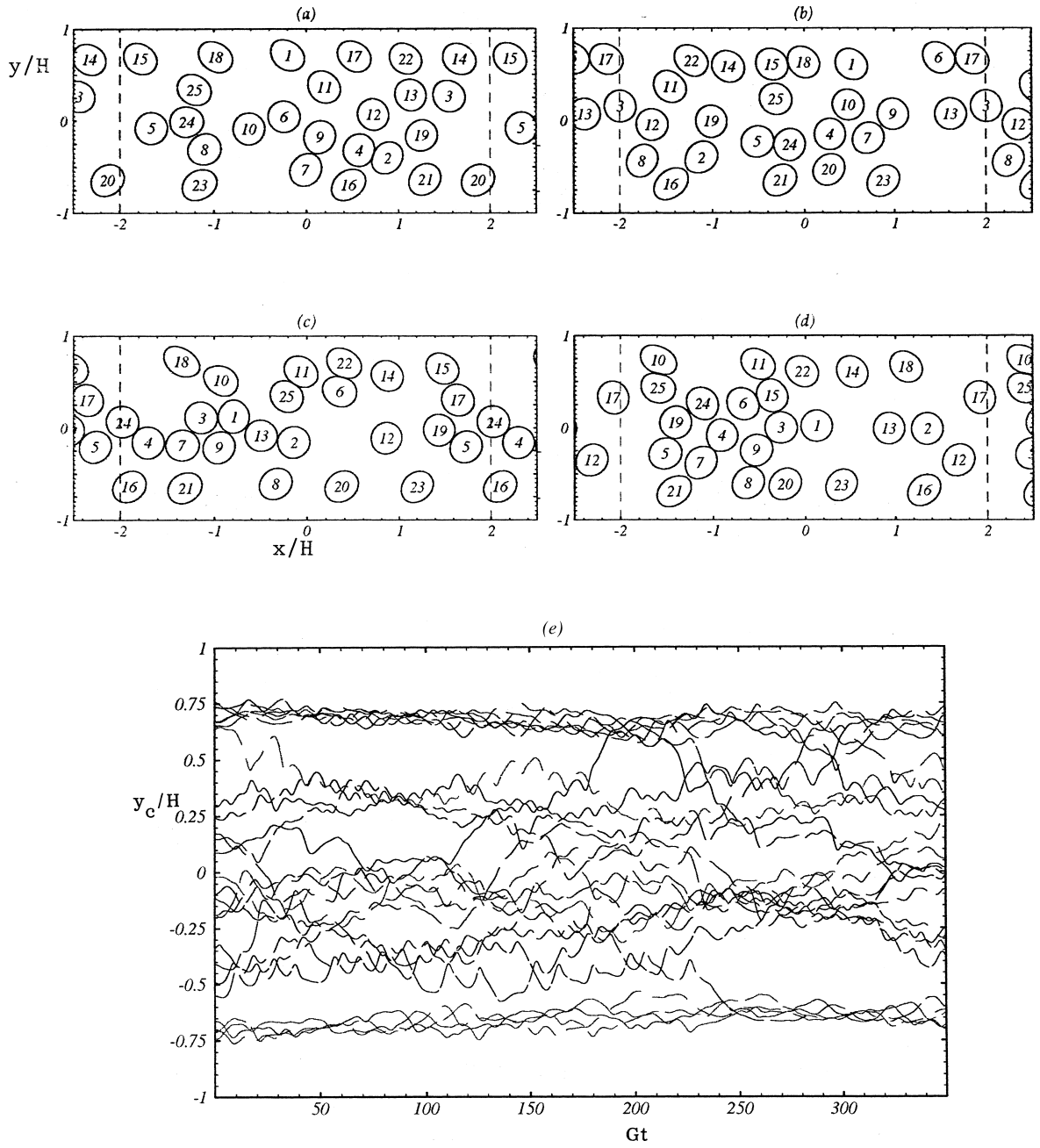

Fig. 7. Simulation of the motion of a suspension of two-dimensional liquid drops in a channel for $\lambda = 1$, $Ca = 0.0866$. (a–d) Instantaneous drop profiles at dimensionless times $\hat{t} = 100$, 200, 300, 350. (e) Evolution of the lateral position of the drop centroids. (f, g) Drop number density distribution and velocity profile averaged over the simulation time after equilibration. (h) The solid line shows the evolution of the relative effective viscosity of the suspension, and the dashed line shows the mean deformation of the drops averaged over all drops.

where the dimensionless function F takes values on the order of unity. At the capillary number presently considered, the magnitude of the dimensionless diffusivity $\hat{D}_{\mathrm{Eff}}$ is comparable to that of the dimensionless self-diffusivity of a drop in a homogeneous suspension in simple shear flow $\hat{D}_{\mathrm{s}} = D_{\mathrm{s}}/(ka^2)$, where k is the shear rate (Li et al., 1996).

A corresponding simulation for $\lambda = 1$, but at the lower capillary number $Ca = 0.0866$, reveals that reducing the deformability of the drops has a significant influence on several features of the motion. Fig. 7(a)–(d) illustrate typical stages in the evolution of the suspension at reduced times $\hat{t} = 100$, 200, 300, 350. For reasons that will be discussed in the next paragraph, this simulation was carried out for an extended period of time. Comparing Fig. 7(a)–(d) with Fig. 6(a)–(f), we find that the less deformable drops have a pronounced

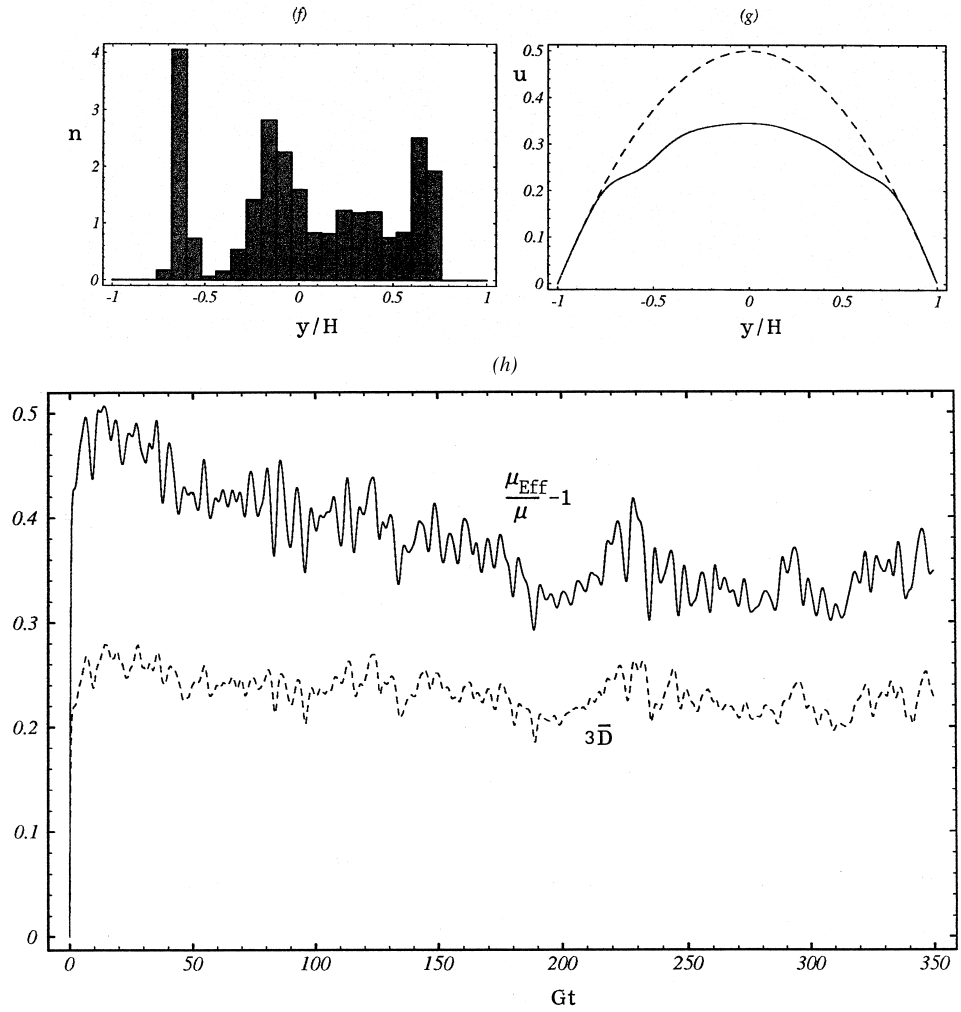

Fig. 7 (*continued*)

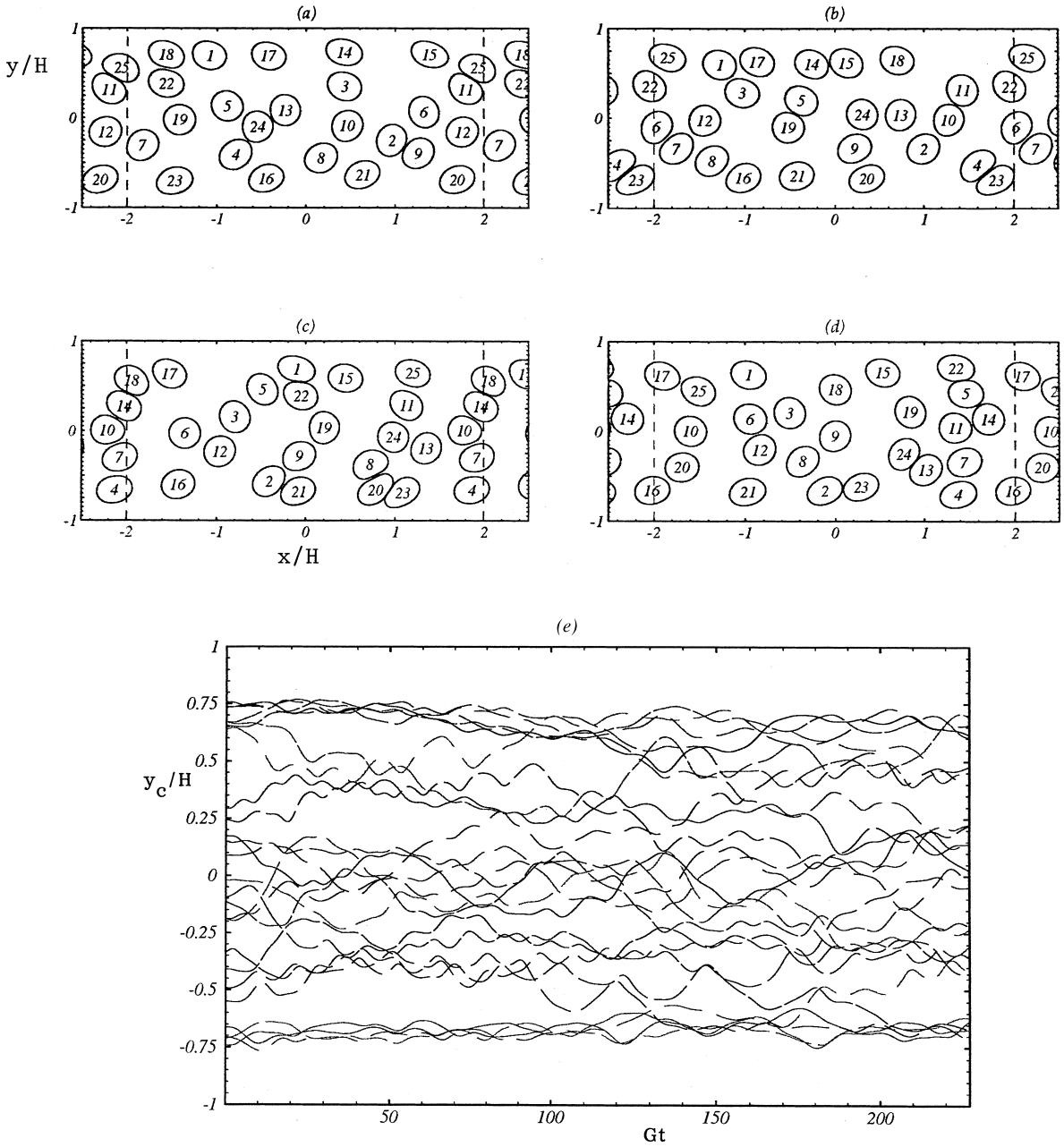

Fig. 8. Simulation of the motion of a suspension of two-dimensional liquid drops in a channel for $\lambda = 10$, $Ca = 0.1732$. (a–d) Instantaneous drop profiles at dimensionless times $\hat{t} = 60$, 115, 170, 225. (e) Evolution of the lateral position of the drop centroids. (f, g) Drop number density distribution and velocity profile averaged over the simulation time after equilibration. (h) The solid line shows the evolution of the relative effective viscosity of the suspension, and the dashed line shows the mean deformation of the drops averaged over all drops.

Table 1
Average properties of a suspension of liquid drops[a]

λ	Ca	Averaging time period $\hat{t}$	$\overline{\mu_{\mathrm{Eff}}}/\mu$	$\hat{t}_{\mathrm{Eq}}$	$\langle \bar{D} \rangle$
1	0.1732	(90, 200)	1.311 ± 0.04	90	0.145 ± 0.09
1	0.0866	(260, 350)	1.338 ± 0.03	260	0.074 ± 0.07
10	0.1732	(150, 225)	1.469 ± 0.04	130	0.123 ± 0.08

[a] An over-bar indicate time average, and angular brackets indicate average over all drops.

tendency to form aggregates separated by solitary drops. Fig. 7(e) shows the evolution of the lateral position of the drop centroids, revealing some unusual activity with drops joining and leaving the two layers of wall drops. Fig. 7(f) displays the drop center number density

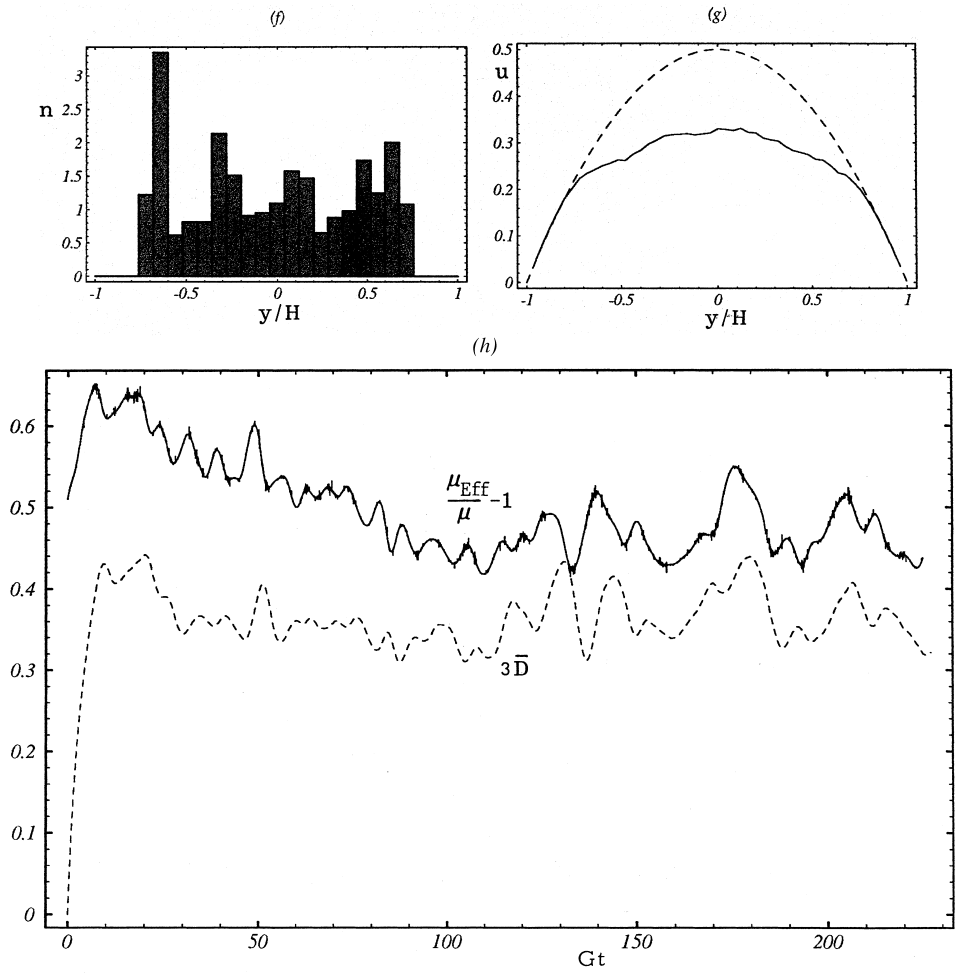

Fig. 8 (*continued*)

distribution averaged with respect to $\hat{t}$ over the interval (260, 350), and Fig. 7(g) displays the average velocity profile. The general features of the distributions shown in these graphs are similar to those discussed earlier for the higher capillary number.

Fig. 7(h) displays the evolution of the suspension effective viscosity and average drop deformation. A comparison with Fig. 6(j) reveals that the oscillations have smaller periods and larger amplitudes compared to those for $Ca = 0.173$. In the present case, the time required for the motion to reach statistical equilibration has been increased to $\hat{t}_{\mathrm{Eq}} = 260$, and this is the reason that the simulation was carried up to the extended time $\hat{t} = 350$. The long equilibration time is due to the slow migration of the drops away from the walls. In this case, the dimensionless effective diffusivity, defined just before Eq. (24), has the value $\hat{D}_{\mathrm{Eff}} = 0.0038$. A comparison with previous results for $Ca = 0.1732$ shows that $\hat{D}_{\mathrm{Eff}}$, and thus the dimensionless function F introduced in Eq. (24), is reduced as the capillary number is lowered while the volume fraction and the viscosity ratio are held constant. This trend contrasts with that of the self-diffusivity in infinite shear flow, as reported by Li et al. (1996). The difference underlines the importance of the walls.

Table 1 compares the equilibration times, the deformation parameter of the drops averaged over all drops and over time after equilibration, and the average effective viscosity; time averages are denoted by an over-bar. Inspection of the effective viscosity reveals a weak shear-thinning behavior which may be attributed, in part, to the pronounced peak of the drop number density distribution near the centerline.

The effect of the dispersed-phase viscosity on the flow of a homogeneous suspension was studied by Charles and Pozrikidis (1998). Their simulations showed that as the viscosity of the drops is raised, lubrication forces developing between intercepting pairs become increasingly important, and this has significant consequences on the dynamics of the microstructure. Fig. 8(a)–(d) illustrate typical stages in the evolution of the suspension in channel flow, for $\lambda = 10$ and $Ca = 0.1732$, at reduced times $\hat{t} = 60$, 115, 170, 225. A comparison with the instantaneous profiles shown in Fig. 6(a)–(f) confirms that as the viscosity ratio is raised, the deformation of the individual drops is reduced, and the particles tend to form clusters.

Fig. 8(e) illustrates the evolution of the lateral position of the drop centroids. Note that two drops that are initially located near the centerline join the bottom layer, while one drop initially belonging to the upper layer enters the bulk of the flow. Comparison with Fig. 6(g) reveals that the viscosity ratio plays a significant role in the nature of the drop trajectories. Fig. 8(f) displays the drop center number density distribution averaged with respect to $\hat{t}$ over the interval (150, 225), and Fig. 8(g) displays the average velocity profile. A comparison with Fig. 6(h) confirms the significant effect of the viscosity ratio; wall peaks are still present, but the distribution over the central region of the channel is somewhat more irregular. The velocity profiles of low and high viscosity drops show only mild differences.

Fig. 8(h) shows the evolution of the suspension effective viscosity μ_{Eff} and average drop deformation. The former was computed by expressing the flow due to each drop in terms of a single-layer potential, and then evaluating the induced flow rate in terms of an interfacial integral (Pozrikidis, 1992). The dimensionless time necessary for the suspension to reach statistical equilibration is $\hat{t}_{\mathrm{Eq}} = 130$, which is higher than that for drops with $\lambda = 1$ at the same capillary number. In addition, fluctuations in the average drop deformation are less well

correlated with those for the effective viscosity than for $\lambda = 1$. The time-averaged values of the effective viscosity and mean drop deformation are shown in Table 1.

Nott and Brady (1994), Fig. 2, tabulated the properties of suspensions of solid spheres deduced by numerical simulation. For volume fraction 0.4 and with 51 particles per unit box, they report the equilibration time $\hat{t}_{\mathrm{Eq}} = 300$, which is nearly twice the equilibration time for two-dimensional drops with $\lambda = 10$ at the areal fraction 0.2945. The effective viscosity of the suspension of rigid spheres is equal to 2.37 μ, which is also substantially higher than the value 1.47 μ corresponding to the suspension of liquid drops. Nott and Brady (1994), Table 1, also report results at the volume fraction 0.3, although in the presence of short-range inter-particle repulsive forces. The effective viscosity lies in the range of 1.62–1.89 μ, which is in good agreement with our results for viscous drops.

5. Discussion

We have found that, in the context of Stokes flow and in the limit of infinite dilution, the integral defining the self-diffusivity of two-dimensional drops in an infinite suspension is divergent. In contrast, the corresponding integral defining the self-diffusivity of three-dimensional drops or rough spheres is convergent. The source of this irregular behaviors has been traced to the slow decay of perturbations in Stokes flow: the absence of inertia allows for far-reaching hydrodynamic interactions. The presence of a confined channel closed container diminishes the intensity of the hydrodynamic interactions by absorbing the leading-order contribution to the flow generated by a particle, but the diffusivity is a strong function of the distance from the nearest wall. The case of spherical rigid particles is special because, even though hydrodynamic interactions are far reaching, the symmetry of the particle shape prevents a non-zero net displacement after a pairwise interception. Wang et al. (1998) computed the gradient diffusivity of spherical particles in a dilute suspension by considering three-particle interactions, and found that, in order for the integral defining the gradient diffusivity to converge, dual renormalization is necessary. A similar renormalization is possible in the case dilute suspensions of two-dimensional drops, but the loss of generality suggests that character of the motion depends on the macroscopic boundary conditions, which is unsatisfying.

A number of previous simulations presented strong evidence that the random motion of rigid or deformable particle in non-dilute two- or three-dimensional homogenous suspensions follow the rules of regular diffusion. Numerical evidence for gradient diffusion has not been presented, apart from the observation that the predictions of phenomenological modeling based on it are in fair agreement with the results of numerical simulations. It appears that the intensity of hydrodynamic particle interactions in a non-dilute suspension is attenuated by the presence of intervening particles, and that hydrodynamic screening promotes a diffusive motion.

The flow of suspensions of rigid spheres is amenable to phenomenological modeling that leads to a convection–diffusion equation for the particle number density distribution. Two approaches have been developed: one relating the particle flux to the local gradients of the particle number density, shear rate, and suspension effective viscosity (Leighton and Acrivos,

1987); and the second based on a suspension force balance (Nott and Brady, 1994). Both approaches may be generalized to suspensions of liquid drops provided that additional fluxes are introduced to account for the effects of particle deformation.

Acknowledgements

This research was supported by the National Science Foundation. Acknowledgment is made to the Donors of the Petroleum Research Fund, administered by the American Chemical Society, for partial support.

References

Batchelor, G.K., 1972. Sedimentation in a dilute dispersion of spheres. J. Fluid Mech 52, 245–268.
Charles, R., Pozrikidis, C., 1998. Effect of the dispersed phase viscosity on the simple shear flow of suspensions of liquid drops. J. Fluid Mech 365, 205–233.
Coulliette, C., Pozrikidis, C., 1998. Motion of liquid drops through tubes. J. Fluid Mech 358, 1–28.
da Cunha, F.R., Hinch, E.J., 1996. Shear-induced dispersion in a dilute suspension of rough spheres. J. Fluid Mech 309, 211–223.
Durlofsky, L.J., Brady, J.F., 1989. Dynamic simulation of bounded suspensions of hydrodynamically interacting particles. J. Fluid Mech 200, 39–67.
Guido, S., Simeone, M., 1998. Binary collision of drops in simple shear flow by computer-assisted video optical microscopy. J. Fluid Mech 357, 1–20.
Hampton, R.E., Mammoli, A.A., Graham, A.L., Tetlow, N., 1997. Migration of particles undergoing pressure-driven flow in a circular conduit. J. Rheol 41, 621–640.
Han, C.D., King, R.G., 1980. Measurement of the rheological properties of concentrated emulsions. J. Rheol 24, 213–237.
Hiller, W., Kowalewski, T.A., 1987. An experimental study of the lateral migration of a droplet in a creeping flow. Exper. Fluids 5, 43–48.
Kennedy, M.R., Pozrikidis, C., Skalak, R., 1994. Motion and deformation of liquid drops and the rheology of dilute emulsions in simple flow. Comp. and Fluids 23, 251–278.
Koch, D.L., 1989. On hydrodynamic diffusion and drift in sheared suspensions. Phys. Fluids A 1, 1742–1745.
Koh, C.J., Hookham, P., Leal, L.G., 1994. An experimental investigation of concentrated suspension flows in a rectangular channel. J. Fluid Mech 266, 1–32.
Kowalewski, T.A., 1980. Velocity profiles of suspension flowing through a tube. Arch. Mech 32, 857–865.
Kowalewski, T.A., 1984. Concentration and velocity measurements in the flow of droplet suspensions through a tube. Exper. Fluids 2, 213–219.
Kwak, S., Pozrikidis, C., 1998. Adaptive triangulation of evolving, closed or open surfaces by the advancing-front method. J. Comp. Phys. 145, 61–68.
Li, X., Charles, R., Pozrikidis, C., 1996. Simple shear flow of suspensions of liquid drops. J. Fluid Mech 320, 395–416.
Leighton, D., Acrivos, A., 1987. The shear-induced migration of particles in concentrated suspensions. J. Fluid Mech 181, 415–439.
Loewenberg, M., Hinch, E.J., 1997. Collision of two deformable drops in shear flow. J. Fluid Mech 338, 299–315.
Morris, J.F., Brady, J.F., 1998. Pressure-driven flow of a suspension: buoyancy effects. Int. J. Multiphase Flow 24, 105–130.
Nott, P.R., Brady, J.F., 1994. Pressure-driven flow of suspensions: simulation and theory. J. Fluid Mech 275, 157–199.

Pozrikidis, C., 1992. Boundary Integral and Singularity Methods for Linearized Viscous Flow. Cambridge University Press, Cambridge.

Rief, F., 1965. Fundamentals of Thermal and Statistical Physics. McGraw-Hill, New York.

van Kampen, N.G., 1981. Stochastic Processes in Physics and Chemistry. North-Holland, Amsterdam.

Wang, Y.R., Mauri, R., Acrivos, A., 1996. The transverse shear-induced liquid and particle tracer diffusivities of a dilute suspension of spheres undergoing a simple shear flow. J. Fluid Mech 327, 255–272.

Wang, Y.R., Mauri, R., Acrivos, A., 1998. Transverse shear-induced gradient diffusion in a dilute suspension of spheres. J. Fluid Mech 357, 279–287.

Young, W.R., 1994. Spatially varying diffusivities and inhomogeneous random walks. Scripps Institution of Oceanography Research Manuscript.

Zhou, H., Pozrikidis, C., 1993a. The flow of suspensions in channels: single files of drops. Phys. Fluids A 5 (2), 311–324.

Zhou, H., Pozrikidis, C., 1993b. The flow of ordered and random suspensions of liquid drops in a channel. J. Fluid Mech 255, 103–127.

Zhou, H., Pozrikidis, C., 1994. Pressure-driven flow of suspensions of liquid drops. Phys. Fluids 6, 80–94.